

IONIZATION IN DIRECT FREQUENCY COMB
SPECTROSCOPY

by

BACHANA LOMSADZE

B.S., Tbilisi State University, Georgia, 2007

AN ABSTRACT OF A DISSERTATION

submitted in partial fulfillment of the
requirements for the degree

DOCTOR OF PHILOSOPHY

Department of Physics
College of Arts and Sciences

KANSAS STATE UNIVERSITY

Manhattan, Kansas

2012

Abstract

Direct frequency comb spectroscopy (DFCS) is currently the highest resolution, absolute frequency spectroscopic technique known. In general, one does DFCS by scanning the repetition rate, f_{rep} , of a comb laser and measuring fluorescence from the excited states of the specie under study. The technique has already been successfully characterized by a theoretical model that starts with the optical Bloch equations and, with a few simplifying assumptions converts them into linear coupled iterative equations. In the present work we build on that successful model to predict the characteristics of the ion yield from photoionization by the comb laser, as a function of f_{rep} . We show that the ion spectrum yields the same atomic structure as the fluorescence spectra, but with greater efficiency. Here, we also set up an experiment and test this theory by measuring the ion signal from direct frequency comb spectroscopy. Furthermore, instead of actively controlling the frequency comb parameters, we allow them to drift, passively measuring them and the ion signal simultaneously. The experiments were found to be in agreement with theory, and the passive comb approach was found to be functional, though not as convenient as the conventional active comb.

IONIZATION IN DIRECT FREQUENCY COMB
SPECTROSCOPY

by

BACHANA LOMSADZE

B.S., Tbilisi State University, Georgia, 2007

A DISSERTATION

submitted in partial fulfillment of the
requirements for the degree

DOCTOR OF PHILOSOPHY

Department of Physics
College of Arts and Sciences

KANSAS STATE UNIVERSITY

Manhattan, Kansas

2012

Approved by:

Major Professor
Brett D. DePaola

Copyright

BACHANA LOMSADZE

2012

Abstract

Direct frequency comb spectroscopy (DFCS) is currently the highest resolution, absolute frequency spectroscopic technique known. In general, one does DFCS by scanning the repetition rate, f_{rep} , of a comb laser and measuring fluorescence from the excited states of the specie under study. The technique has already been successfully characterized by a theoretical model that starts with the optical Bloch equations and, with a few simplifying assumptions converts them into linear coupled iterative equations. In the present work we build on that successful model to predict the characteristics of the ion yield from photoionization by the comb laser, as a function of f_{rep} . We show that the ion spectrum yields the same atomic structure as the fluorescence spectra, but with greater efficiency. Here, we also set up an experiment and test this theory by measuring the ion signal from direct frequency comb spectroscopy. Furthermore, instead of actively controlling the frequency comb parameters, we allow them to drift, passively measuring them and the ion signal simultaneously. The experiments were found to be in agreement with theory, and the passive comb approach was found to be functional, though not as convenient as the conventional active comb.

Table of Contents

Table of Contents	vi
List of Figures	viii
Acknowledgements	xiv
Dedication	xv
Preface	xv
1 Introduction	1
1.1 Frequency Combs and Their Application	1
1.2 Direct Frequency Comb Spectroscopy	5
1.3 Motivation	7
1.4 Ion Detection vs Photon Detection	7
1.5 Dissertation Overview	8
2 Theoretical Modeling and Calculations	9
2.1 Felinto Model	9
2.2 Our Model	11
2.3 Theoretical Results	14
2.4 Additional Results	16
3 Experimental Setup	25
3.1 Target System	25
3.1.1 Laser locking	29
3.2 Ion Detection	33

3.3	Experimental Setup for DFCS	34
3.3.1	Measuring f_{rep} and f_{off}	35
3.3.2	Our experimental scheme	37
3.3.3	Stability of the laser and range of f_{rep} and f_{off}	42
3.4	Data Acquisition	46
4	Experimental Results	48
4.1	Binned 2D Plot of Our Experimental Results	48
4.2	1D Plot in Comparison with Theory	49
5	Conclusion and Future Possibilities	53
5.1	Summary	53
5.1.1	Theory	53
5.1.2	Experiment	55
5.2	Future Possibilities	56
	Bibliography	61
A	Estimating the Laser Beam Size	62
B	Labview Program for Data Acquisition	64
C	Binning-Program	67
D	Identifying Structure Lines	80
D.1	Two Photon Transition	80
D.2	One Photon Transition	87
E	External Cavity Diode Laser	93
F	Moving MOTRIMS	96

List of Figures

- 1.1 This graph shows a frequency comb in the time domain. It represents a train of an infinite number of pulses separated from each other by constant time $T = 1/f_{rep}$ and having constant phase slip φ_{cep} from pulse to pulse. 3
- 1.2 This is the Fourier transform of the pulse train of Fig. 1.1, it consists of very sharp lines called “teeth” separated by the repetition frequency of the laser, f_{rep} . Because of the phase shift between the pulse envelope and carrier (φ_{cep}), the “zeroth” tooth doesn’t start from 0 Hz but is shifted by an amount called the offset frequency f_{off} 4
- 2.1 Simplified energy level diagram for ^{87}Rb . Individual states are grouped into manifolds. The continuum is modeled by manifolds 4 and 5. See text for details. 13
- 2.2 Plot of the relative populations in the $5p$, $5d$ and Rb^+ manifolds as functions of the comb laser repetition frequency, minus a fixed reference frequency, $f_{ref} = 75557551$ Hz. The $5p$ population is plotted as round points connected by a line (green) and uses the linear scale on the far right; the $5d$ population is plotted as a solid line without points (red) and uses the log scale on the left; the Rb^+ population is plotted as crosses connected by a line (blue) and also uses the log scale on the left. All of the peaks in the $5d$ and ion curves have been identified as resulting from 2-photon transitions from the $5s \rightarrow 5d$ manifolds. A few selected peaks are labeled as (1) $5s_{1/2}, F = 1 \rightarrow 5d_{5/2}, F = 2$; (2) $5s_{1/2}, F = 2 \rightarrow 5d_{5/2}, F = 2$; (3) $5s_{1/2}, F = 1 \rightarrow 5d_{5/2}, F = 1$; (4) $5s_{1/2}, F = 2 \rightarrow 5d_{5/2}, F = 4$ 15

2.3	Computation of $5d$ (solid line without points, red) and ionization (solid line with crosses, blue) manifolds under the artificial initial condition that the initial population of $5p$ states (solid line with circular points, green) varies sinusoidally with f_{rep} . The ionization population largely follows the $5d$ population. However, the lack of $5d$ structure in the ionization population is an indication of 2-photon ionization of states in the $5p$ manifold (without being resonant with an intermediate $5d$ state.)	18
2.4	Detail of $5p$ population for low and high intensity comb laser. The peak near 7 Hz is from the $5s_{1/2}, F = 2 \rightarrow 5p_{3/2}, F = 2$ transition and clearly shows the effects of optical pumping. The peak near 15 Hz is from the $5s_{1/2}, F = 2 \rightarrow 5p_{3/2}, F = 3$ transition, for which no optical pumping is expected. The two curves were scaled such that the peaks near 15 Hz had the same magnitude.	19
2.5	Ground state hyperfine populations versus f_{rep} when a comb tooth is resonant with the $5s_{1/2}, F = 2 \rightarrow 5p_{3/2}, F = 2$ transition. (a) is for low comb laser intensity and does not exhibit strong optical pumping. In (b) the comb laser intensity is high and strong optical pumping from $5s_{1/2}, F = 2$ to $5s_{1/2}, F = 1$ is clearly seen. (c) and (d) are the same intensity conditions as (a) and (b), respectively, but f_{off} has been adjusted such that a second comb tooth is resonant with the $5s_{1/2}, F = 2 \rightarrow 5p_{3/2}, F = 2$ transition. The optical pumping is minimal, as expected.	20
2.6	This is a plot of two particular states' populations as a function of chirp parameter. The blue curve on the graph is a so-called Type A transition (see text for details) and the red curve is a Type B transition.	21

2.7	The same as Fig. 2.2, but for 50 pulses in the train. The peaks are slightly broader and “ringing” is seen in the populations. The ringing is real, and is actually due to the Fourier transform of a rectangular pulse, superimposing a sinc function on the comb teeth, and is especially evident on the $5d$ curve.	24
3.1	Hyperfine structure of $5s_{1/2}$ and $5p_{3/2}$ states of Rb atoms. The solid red arrow pointing up shows trapping transition red detuned from resonance. The solid red arrow pointing down and the dashed blue arrow show the decay possibilities.	27
3.2	Hyperfine structure of $5s_{1/2}$ and $5p_{3/2}$ states of Rb atoms. Solid red arrow pointing up shows repump transition.	28
3.3	Schematic of saturated absorption setup for the repump laser; M-Mirror, BS-Beam Splitter.	29
3.4	Hyperfine structure of Rb $5s_{1/2}$ and $5p_{3/2}$ including (1-2) and (2-3) crossover “states”.	31
3.5	Schematic of saturated absorption setup for the trapping laser; M-Mirror, BS-Beam Splitter, $\lambda/4$ (quarter) wave plate.	32
3.6	Recoil Ion Momentum Spectrometer used for collecting the ions. Anti-Helmholtz coils are for the MOT. Ions produced inside the trapping chamber are extracted with the electric field applied on the spectrometer and directed onto a recoil ion detector.	33
3.7	Simplified schematic of an oscillator. It consists of a couple of prisms, a crystal, an output coupler and a pump laser.	34
3.8	Schematic for measuring f_{rep} and f_{off} . Pulses coming from the oscillator are split in half with a 50/50 beam splitter; half goes to f-2f interferometer and half goes to another beam splitter, 10% of which is used to read f_{rep} and the rest is sent to the MOT chamber.	36

3.9	Schematic of an f-2f interferometer; PCF-Photonic Crystal Fiber, DBS-Dichroic Beam Splitter, PBS- Polarized Beam Splitter. Pulses from the oscillator are sent through the PCF. It generates an octave in the laser spectrum. Then using the DBS, the pulses are split. The lower frequency components are transmitted and frequency doubled using a BBO crystal. The higher frequency components are reflected and sent to the delay stage. Later on these two arms are combined and a beat frequency is measured.	38
3.10	Spectra of the pulses before (top) and after (bottom) the PC Fiber. The lower spectrum covers an octave as it has 532 and 1064 nm photons in it. . .	39
3.11	Idea behind the f-2f interferometer. The spectrum shown above covers an octave as it has frequencies f_n and f_{2n} . Using a BBO crystal, the f_n component is frequency doubled and beat against f_{2n} . The beat frequency is the difference between the components and as is shown above, it is f_{off}	40
3.12	Experimental scheme for DFCS. The pulses from the oscillator were sent to the MOT and the ions produced inside the chamber were counted simultaneously with f_{rep} and f_{off}	41
3.13	This is the same setup as Fig. 3.12, but with no ion detection. Pulses were split in half. 50% was sent to the f-2f interferometer for the f_{off} measurement, and the rest was sent to a fast photo-detector for the f_{rep} measurement. . .	43
3.14	This is a plot to demonstrate how f_{off} and f_{rep} change in time. In this case only 2 hours of data are presented.	44
3.15	This is a plot to estimate how stable f_{off} and f_{rep} are in different sampling times. The calculation below the figure was done for a 1 second sampling time.	45
3.16	Data acquisition scheme. Signals from f_{off} and f_{rep} counters were sent to the computer through a GPIB-USB converter. The ion signal from the PSD was read in through the CFD-NI DAQ.	47

4.1	Plot of rubidium ion count rate, in ions per 100 ms, as a function of the freely varying parameters f_{rep} and f_{off} . $f_{\text{ref}} = 75616231$ Hz.	50
4.2	The data from Fig. 4.1 (solid black line). The ion count rates have been averaged over the cycles in f_{rep} and f_{off} and plotted versus $f_{\text{rep}} - f_{\text{ref}}$, where $f_{\text{ref}} = 75616232$ Hz. Also plotted is the calculated ion signal rate (crosses connected by a line). For both theory and experiment $f_{\text{off}} = -23.5$ MHz.	52
A.1	Here we estimate size of the beam using the so-called knife-edge method. The black line is data, and the red line is a fitted Gaussian.	63
B.1	LabView code1.	65
B.2	LabView code2.	66
E.1	Home-made external cavity diode laser 1.	94
E.2	Home-made external cavity diode laser 2.	95
F.1	This is how the MOTRIMS apparatus looks after we moved into the new room.	97

Acknowledgments

I would like to thank a lot of people for their help, support and advice in completing this work.

First of all I am very grateful to my advisor Professor Brett DePaola. He is an outstanding mentor and teacher. One of the many reasons I chose him to be my advisor was the care and attention with which he guided his prior students, during and after their PhD's. He was always with us in the lab; if I had any problems I didn't need to make an appointment with him to ask him a question; he was just right next to us all the time. In the beginning of my research I remember I didn't know much about the electronics and lasers. His idea was that if you want to be an experimentalist you need to stop thinking about the electronics as just being black boxes and lasers just something that lases and start understanding how they work. He taught me how to design and built my own electronic circuits and he helped me build an external cavity diode laser. I never felt uncomfortable working with him, as he knows how to communicate with students. He is very friendly and always very patient even when explaining things that seem trivial now. And during my PhD he gradually built my confidence. That is exactly the sign of an excellent mentor. He is a big source of advice and knowledge, not only in physics but outside as well. His advice was always extremely helpful and the decisions I have made based on them have always led to success.

I'd also like to thank Dr. Charles Fehrenbach. He was my second advisor. When Brett was not in town and I had beamtimes Charles with his genius ideas was there with me. His comments and suggestions on my experimental and theoretical work were always very helpful.

Former student Dr. H. Jang: He was my lab partner in the beginning of my project.

Outside the group; I would like to thank Professor Larry Weaver for many extremely helpful discussions.

Dr. Daniel Felinto for the generous donation of his computer code that served as the starting point from which our theoretical model evolved.

The experts in the field of my research: Professors Brian Washburn and Kristin Corwin for their very helpful advice.

Their former student Dr. Jinkang Lim: I enjoyed discussions about frequency combs with him very much.

Vince Needham for the data acquisition software.

I would face a lot of problems while working on my PhD without my prior physics knowledge and lab. Skills that I received at Tbilisi State University (in Georgia). I would like to thank all my professors for giving me the education that was the starting point for my PhD.

And last but not least my parents and my sister. It was very hard for me to be very far away from them, but their continuous love and support made me strong and stay motivated. Thank you and I love you.

Thank you all for your individual help.

Dedication

To my parents.

Chapter 1

Introduction

High precision/sensitivity measurements are, and always have been, of interest in the sciences, partly because of the wide practical application. Despite incremental progress, the measuring precision of the spectral properties of materials had been limited by the resolution and range of the measuring tools themselves, until roughly a decade ago when the optical frequency comb was developed. Frequency combs have revolutionized atomic molecular and optical physics. They have made it possible to determine standards of fundamental quantities of time, frequency and length.^{1,2} Nowadays they are used in many fields, from doing spectroscopy of atomic and molecular systems, to biology, and to medicine.³⁻⁹ Scientists from all over the world have been conducting research using frequency combs. Our group is also part of this big community. The work presented in this dissertation is about estimating the ionization rate in Direct Frequency Comb Spectroscopy.

1.1 Frequency Combs and Their Application

In general frequency combs are described in the frequency domain, partly because it is easy to visualize and partly because most of the research involving frequency combs is carried out in the frequency domain.

But if one wants to study the physics behind the interaction between the comb and the target system it is useful to look at the combs in the time domain. Here we briefly review both representations.

Let's imagine that we have a Ti:Sapphire femto-second oscillator¹⁰ that operates with a repetition frequency of 80 MHz. In the time domain that means that the time separation between pulses is about 12.5 ns. In addition to this, these pulses differ from each other by a phase called the carrier envelope phase (CEP). Because of temperature fluctuations or small ground vibrations, the time difference between pulses and the phase jump from pulse to pulse change in time. Using fast responding servo electronics one can manage to keep these parameters stable. Then mathematically the output of the oscillator can be written as:

$$E(t) = \sum_{n=0}^{\infty} E_0 \cdot e^{-\frac{\ln(2)(t-nT)^2}{\tau^2}} e^{i(\omega_c t - n\omega_c T)} e^{in\varphi_{cep}} e^{i\varphi_o} \quad (1.1)$$

where E_0 is the peak electric field of the pulses, T the time separation between pulses, τ is the full width at half maximum (FWHM) of the pulse duration, ω_c is the carrier frequency of the laser, φ_{cep} is the phase jump from pulses to pulse, and φ_o is the initial constant phase between the envelope of the pulse and the carrier

So, a frequency comb is nothing but a train of an infinite number of pulses whose time separation and CEP are locked. See Fig. 1.1.

Now if we take the Fourier transform of Eq. 1.1 we will get the frequency representation of a comb; the spectrum is shown in Fig. 1.2. The spectrum is composed of discrete narrow-band teeth that are separated by the repetition frequency of the laser. The envelope under which the teeth lie is just the Fourier transform of a single pulse in the train. Because of the CEP the comb structure doesn't exactly start from 0 Hz but is shifted from it by the amount called the offset frequency (f_{off}). Mathematically it relates to CEP as $f_{off} = f_{rep}(2\pi\varphi_{cep})^{-1}$

Then the frequency of the n^{th} tooth in the spectrum can be written as

$$f_n = nf_{rep} - f_{off}, \quad (1.2)$$

where n is an integer.

Considering that the FWHM bandwidth of a typical Ti:Sapphire laser is about 100 nm, this gives us about 10^6 teeth within the frequency envelope. This means that if one wants

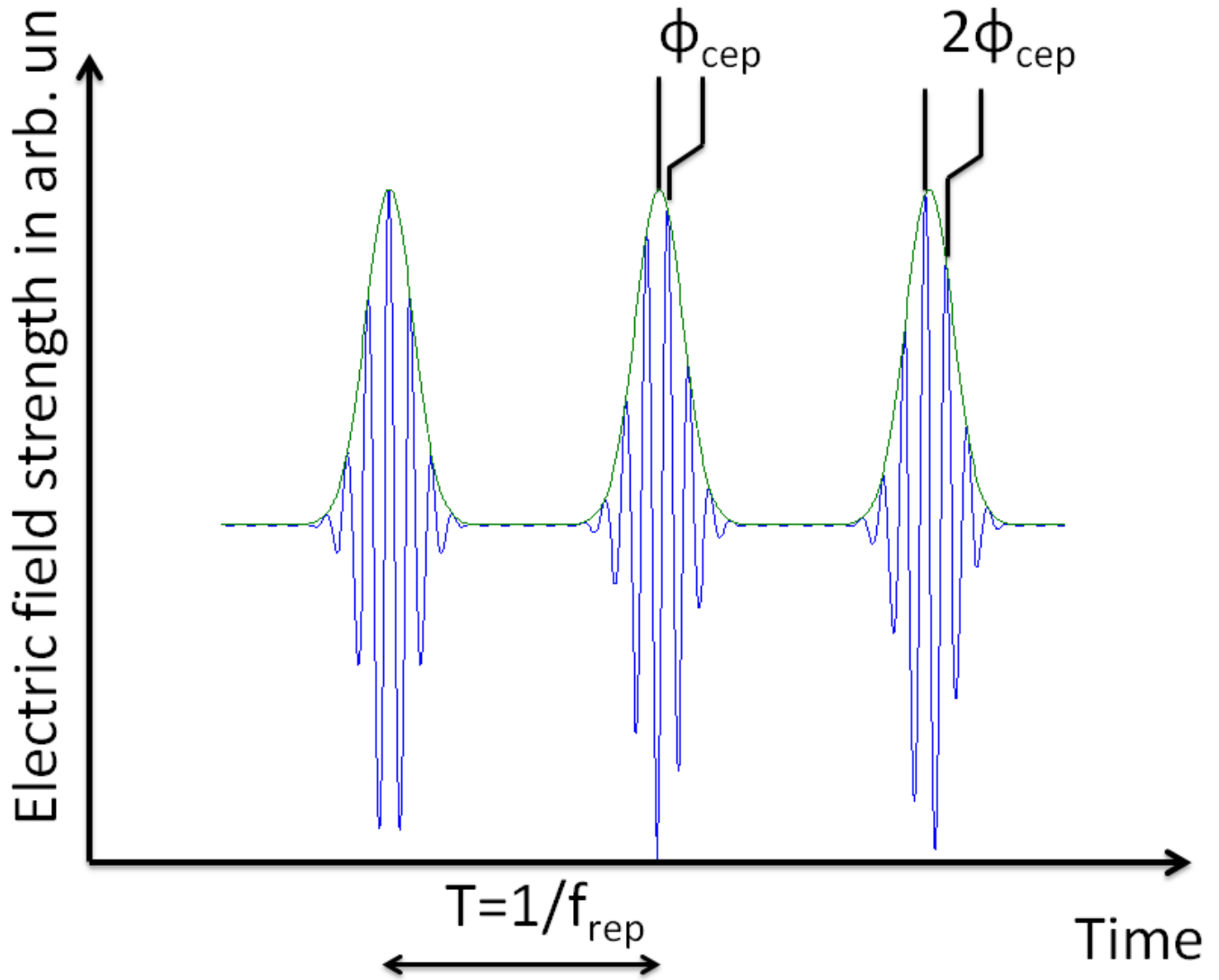


Figure 1.1: *This graph shows a frequency comb in the time domain. It represents a train of an infinite number of pulses separated from each other by constant time $T = 1/f_{rep}$ and having constant phase slip φ_{cep} from pulse to pulse.*

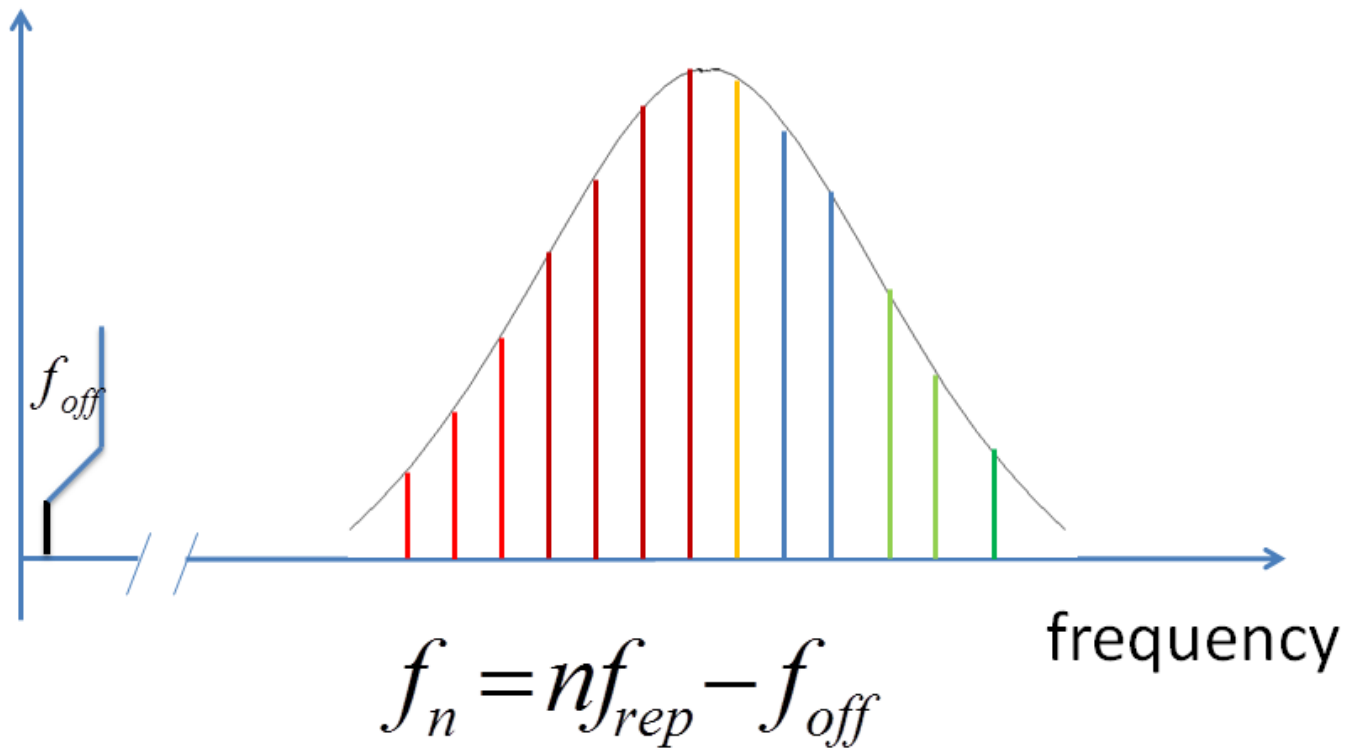


Figure 1.2: This is the Fourier transform of the pulse train of Fig. 1.1, it consists of very sharp lines called “teeth” separated by the repetition frequency of the laser, f_{rep} . Because of the phase shift between the pulse envelope and carrier (φ_{cep}), the “zeroth” tooth doesn’t start from 0 Hz but is shifted by an amount called the offset frequency f_{off} .

to study the structure of a system of interest one has the equivalent of 10^6 well stabilized narrow bandwidth CW lasers available at the same time. That is why the frequency combs are fascinating tools for spectroscopy. For example, using a frequency comb and a newly developed technique called Direct Frequency Comb Spectroscopy (DFCS),^{8,9} one can study the internal structure of atoms, molecules and complicated systems with extremely high precision.

1.2 Direct Frequency Comb Spectroscopy

Direct Frequency Comb Spectroscopy is a powerful, relatively new technique for high-resolution spectroscopy on atomic or molecular systems. There are other spectroscopic techniques that have comparable resolution (10-400 kHz). For example a group¹¹ using a diode laser determined the absolute frequencies of the hyperfine transitions of the Rb two D lines interferometrically by comparison with an $^{127}\text{I}_2$ -stabilized $\text{He} - \text{Ne}$ laser, but they are limited with the scanning range of the diode laser and that limits the transitions one wants to measure. In the case of DFCS the range is not an issue. Using just one frequency comb one can measure the absolute frequencies of many different levels. In general, as was described in many scientific articles,^{8,9,12} one does DFCS by taking a frequency comb, shining it at the system of interest and looking at the excitation signal through fluorescence as one scans either the repetition frequency, f_{rep} , or offset frequency, f_{off} , of the laser. Scanning f_{rep} just means changing the separation between teeth in the frequency domain. So as one scans f_{rep} , every time a tooth becomes resonant with a transition frequency, an excitation can happen. Then, after a decay, the fluorescence signal is detected using a photodiode or photomultiplier. Doing DFCS by scanning f_{off} is very similar. In this case all the comb teeth move as a whole rigid system and again every time a tooth matches a transition frequency in the system, an excited state can become populated, which one detects through the fluorescence.

In the time domain we can understand this process as follows. One pulse (broad band-

width) comes and hits a target system and excites it to an excited state. Before the second pulse comes along this quantum mechanical state evolves in time, and hence picks up some phase. Now if the phase of this state and the phase of the second pulse (shifted by the CEP with respect to the first) constructively interfere, we get an enhancement in excitation.¹³ On the other hand if they interfere destructively, then the excitation is suppressed. The same process happens for the next pulse and every pulse in the train. Basically, the excitation one detects is an effect of accumulated phase. So as one scans either f_{rep} or f_{off} one can study the structure of the system because at one particular f_{rep} or f_{off} only a few states constructively interfere with the laser pulses and for some different f_{rep} or f_{off} other states do.

This technique was first used by Ye's group.^{8,9,12} They used this method to study the structure of ^{87}Rb atoms with very high precision. States of interest were the hyperfine states of the $5s$, $5p$ and $5d$ manifold. Measuring the hyperfine structure of the $5p$ states was done by keeping f_{rep} constant and scanning f_{off} . By doing so, when a comb tooth is shifted into resonance with a transition between states in the $5s$ and $5p$ manifolds, for example from $5s_{1/2}, F = 2$ to $5p_{3/2}, F = 3$, then the upper state ($5p_{3/2}, F = 3$) will be populated, and a fluorescence signal from the $5p$ manifold can be detected.

Perhaps even more interesting, 2-photon excitation can occur when the frequencies of two comb teeth sum to the frequency difference between states *via* a non-resonant transition to an intermediate state. At first, this type of transition seems unlikely, due to the non-resonant character of the intermediate transition. However, as Ye's group has pointed out,⁸ if one pair of teeth is 2-photon resonant, then thousands of other pairs of teeth will also be resonant with that same transition. For example, if f_n and f_m combine to be 2-photon resonant, then so will $f_{n+1} + f_{m-1}$ and $f_{n+2} + f_{m-2}$, etc. That is how the hyperfine structure of the $5d$ states was studied. The important thing to mention here is that with the DFCS method Ye's group measured all the possible transitions in the $5s$, $5p$ and $5d$ states with sub-Hz precision.

1.3 Motivation

DFCS, as we mentioned in the previous section, is done by counting fluorescence photons as one scans f_{rep} or f_{off} . Considering that a frequency comb is a train of femtosecond pulses having high peak intensity, it is reasonable to ask if, in addition to the excitation, do frequency combs also ionize the system? The relevant questions are, “Is the ionization signal negligible? And if the ionization signal is strong enough, can that be used to do DFCS instead of looking at the fluorescence signal?” These are the questions that motivated our work.

In this dissertation we answer these questions both theoretically and experimentally. Having answers to these questions will be very beneficial for theoreticians of course, but it will be even more so for experimentalists for the reasons described in the following section.

1.4 Ion Detection vs Photon Detection

Detecting ions has some advantages. First, ion detection is far more efficient than photon detection: Use of electric fields can give 4π steradian ion collection (if Stark effects from the extraction fields are a problem, the electric field can be pulsed) and quantum detection efficiency (QDE) for ion detectors is typically higher than photon detectors (for example QDE for photomultiplier tubes is about 30%, whereas for ion detectors it is 40-80 %). Furthermore, although in the original experiment⁸ (described in section 1.2) the photons detected after 2-photon excitation were at a different wavelength from the laser, this will not be the case in general. For example if one wants to study the structure of the Rb $4d$ states using two different combs, one comb centered at 780 nm used for excitation from $5s$ to $5p$, and the second centered at 1529 nm for $5p$ to $4d$, the photons resulting from decay will have the same wavelengths as the lasers because the decay and excitation pathways are identical. In contrast, background counts should be negligible in appropriately designed ion detectors.

1.5 Dissertation Overview

This dissertation is divided into 5 chapters.

- In the second chapter we model the continuum states to study the ionization process in DFCS. In the same chapter we show the results of the calculations. While we were calculating the ionization rate we found some very interesting results related to the excitation process and these results are shown below too.
- In the third chapter we describe the construction of an experimental setup to test the results predicted by our newly developed code.
- In the fourth chapter the results of the experiment are shown and compared to the theory.
- In the fifth chapter we summarize our work.

Chapter 2

Theoretical Modeling and Calculations

In this chapter we describe the theoretical model, developed by our group, that was used to calculate the ionization rate in DFCS. The calculation is based on the model by Felinto^{14,15} created for calculating the excitation process in DFCS. This chapter is divided into the following sections:

- In the first section the Felinto model is reviewed.^{14,15}
- In the second section we model the continuum states and incorporate them into the Felinto model.
- In the third section we show the results of our newly developed model.
- In the final section we apply our code to look at the effects of chirp, optical pumping, and the number of pulses in a train on the excitation.

2.1 Felinto Model

The model developed by Felinto calculates the population of ground and excited states of the system of interest after interacting with a train of equally (temporally) spaced pulses, all identical, except for a fixed pulse-to-pulse phase shift, ϕ .

The Felinto model starts with the optical Bloch equations

$$\frac{\partial \rho_{ij}}{\partial t} = -\frac{i}{\hbar} \langle i | [\hat{H}, \hat{\rho}] | j \rangle - \Gamma_{ij} \rho_{ij} + \delta_{ij} \sum_r \gamma_{ij} \rho_{rr}, \quad (2.1)$$

where ρ is the density matrix, \hat{H} is the total Hamiltonian (the Hamiltonian of the field-free system \hat{H}_0 , plus the interaction potential $\hat{V}(t)$), Γ_{ij} is the relaxation rate of the ij component of the density matrix, δ_{ij} is the Kronecker function, and $\sum_r \gamma_{ij} \rho_{rr}$ is the incoherent feeding term of the i^{th} level by the population of all the upper r states. Felinto, uses the Eq. 2.1 to study the excitation of rubidium $5s$, $5p$, and $5d$ manifolds by calculating the diagonal elements of the density matrix. By “manifold” is meant the full structure with fine and hyperfine levels; those 3 manifolds include a total of 16 states when summed over the magnetic quantum number m_F . The Bloch equations are not integrated over the entire interaction time. Rather, the excitation is calculated for a single laser pulse and the effects of multiple pulses are added coherently using an iterative algorithm that includes incoherent redistribution of population by spontaneous decay occurring between pulses.

$$\rho_{ij}^{n+1} = e^{(\omega_{ij} + \Gamma_{ij})T} (\rho_{ij}^n - \frac{i}{\hbar} \int_0^\infty e^{i\omega_{ij}t} \langle i | [\hat{V}^n(t), \hat{\rho}^c] | j \rangle dt + \delta_{ij} \sum_r \gamma_{ir} \int_0^\infty e^{\Gamma_{ir}t} \rho_{rr}(t) dt) \quad (2.2)$$

where $\omega_{ij} = (E_i - E_j)/\hbar$ is the transition frequency between i, j energy levels, and T is the time separation between pulses. This equation gives the population of a state impulsively excited by $(n + 1)^{th}$ pulse in terms of the population of the same state prior to that pulse. In deriving Eq. 2.2 Felinto assumed that the incoherent redistribution of populations (due to spontaneous emission) occurs on a timescale that is long compared to that of coherent excitation. It was also assumed that the time between pulses is long compared to the width of the pulses.

In the formulation developed by Felinto, one can compute the time evolution of the population of each state in all three manifolds to any chosen level of perturbation, at a computation cost that is linear in order of perturbation. In Felinto’s (and our) computer code, computer round-off limits us to 12^{th} order perturbation,¹⁶ which is at the low end of the strong field regime.

2.2 Our Model

For this work we want to include photoionization of the $5d$ states, so two extra manifolds were added to the model: the “continuum”, labeled 4, and “holding” states, labeled 5. The continuum manifold is modeled by 26 discrete energy levels. Each level is composed of 14 energy-degenerate angular momentum states, one for every possible angular momentum required to allow a transition from each of the 8 states in the $5d$ manifold. The 26 discrete levels are spaced 2 THz apart, for a total frequency spread in the manifold of 50 THz (or about 100 nm at the laser’s central wavelength), allowing us to span the bandwidth of the excitation laser. Manifold 4 lies above manifold 3 by an energy equivalent to the central frequency of the comb laser. We are modeling ionization by excitation to the pseudo states that we placed above the ionization potential. All the angular portions of the dipole matrix elements for excitation to the continuum manifold were computed using the usual angular momentum algebra, thereby guaranteeing orthonormality. The reduced matrix element for ionization was estimated using the Rb($5d$) photoionization cross section measured¹⁷ using a cw laser with frequency near that of the center of the comb envelope. The photoionization cross section is expected¹⁷ to vary little over the bandwidth of the comb envelope frequency.

Simply modeling a continuum in this fashion is unsatisfactory because the levels are still discrete and the model would therefore not predict ionization if the photon energies added to something between the discrete levels. Furthermore, states in the continuum manifold must be treated differently from bound states: ions do not spontaneously decay back down to bound states. And while it is possible for an atom excited to the ion continuum to undergo stimulated emission in the same short laser pulse, it is unrealistic to allow electrons ionized with one pulse to be stimulated back down to the bound state with the next pulse, several nanoseconds later.

In order to address these two issues and make our code more realistic we added a 5th manifold to our model, a so-called “holding” manifold. This manifold consists of 18 degenerate states, one for every possible angular momentum required to allow a transition from each

of the continuum states in manifold 4. The single energy of these 18 states was chosen to lie a couple of laser bandwidths below the continuum states and is coupled to the continuum states only through spontaneous emission. The decay rate for the continuum states, Γ , was chosen to be 2 THz. That is, the line width of the “continuum” levels is equal to the spacing between adjacent levels. Furthermore, atoms that are excited to the continuum, decay to the holding manifold on a timescale consistent with a true ionization process. In total, then, 398 discrete states are used to model the Rb atom and its continuum: 2 in manifold 1, 6 in manifold 2, 8 in manifold 3, $14 \times 26 = 364$ in manifold 4, and 18 in manifold 5. A partial energy level diagram of the model ^{87}Rb system is shown in Fig. 2.1. We note that for some purposes this model of the continuum is unsatisfactory. For example, if our goal was to measure the energy distribution of the photoionized electrons, this model would be a poor one, because when an electron is ionized, we have no way of knowing which comb tooth (and consequently what photon energy) was responsible for the ionization. However, for simply counting the number of ionization events, we expect the model to be quite satisfactory.

In the original Felinto model, one of the approximations made was that incoherent redistribution occurs on a timescale that is long compare with that of coherent excitation.¹⁵ Therefore in Eq. 2.2, terms containing Γ_{ij} , the decay rate between levels i and j , could be removed from their integrals and neglected during the pulse. It is clear that in our model for which the Γ 's of the continuum states equal 2 THz, this approximation is no longer valid. Therefore we numerically integrate these terms. The only additional approximation we are making in this model is to ignore excitation to and ionization from the $7s$ states, which could be populated with one photon excitation from the $5p$ states. Justification for this approximation is that the $5p \rightarrow 7s$ transition wavelengths are on the edge of the laser bandwidth of a typical Ti:Sapphire comb laser and correspondingly their contribution to the ionization signal should be negligible. Nevertheless, at some later time it may prove interesting to include the $7s$ states in the calculation to see what role they may play in ion production.

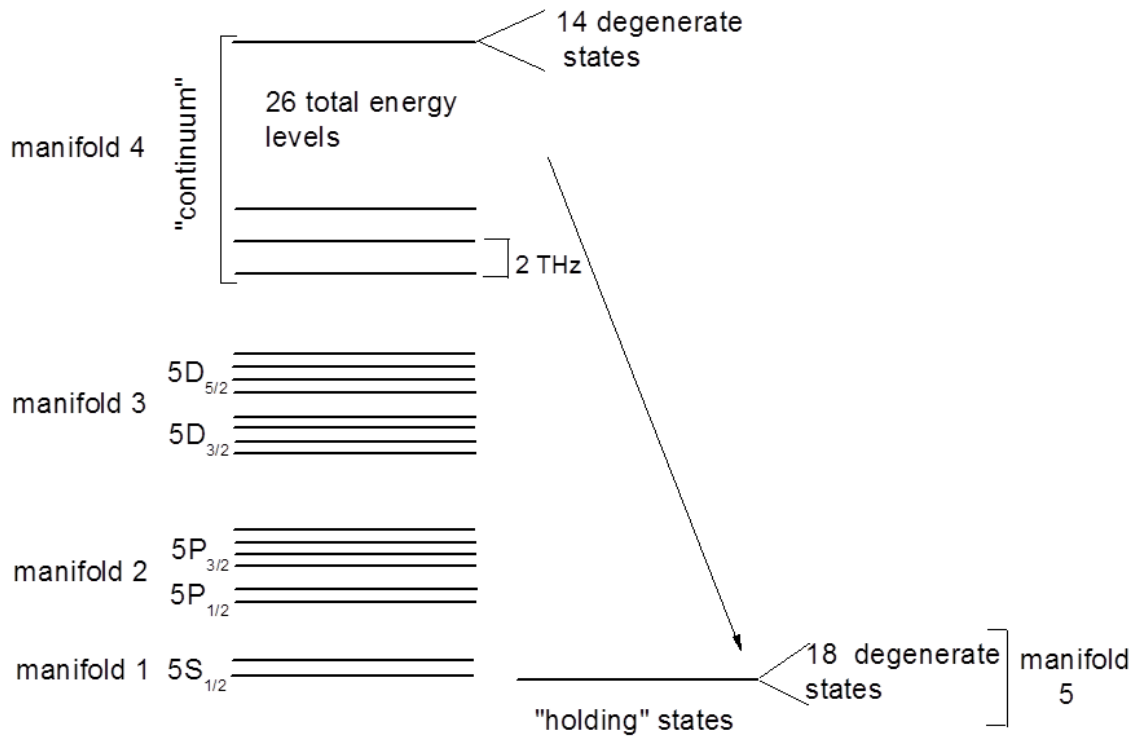


Figure 2.1: *Simplified energy level diagram for ^{87}Rb . Individual states are grouped into manifolds. The continuum is modeled by manifolds 4 and 5. See text for details.*

The initial repetition rate of the comb laser in the computation was 75557551 Hz, which is typical of the comb used in our laboratory. We define this frequency to be f_{ref} . Most calculations were made using 950 pulses in the train. This seems to be a good compromise¹⁵ between the narrowing of the comb teeth that more pulses cause, and broadening of the resonances from the incoherent process of spontaneous emission.

2.3 Theoretical Results

Figure 2.2 shows the result of a typical calculation. Here, relative populations in the $5p$, $5d$, and Rb^+ (continuum plus holding) manifolds are plotted versus $f_{\text{rep}} - f_{\text{ref}}$. Though their heights vary over several orders of magnitude, each peak in the $5d$ and ion curves has been identified as resulting from a specific 2-photon transition between the $5s \rightarrow 5d$ manifolds; a few representative peaks are labeled in the figure. The individual laser pulses were hyperbolic secant, having temporal widths of 50 fs, and peak intensities of 10^4 W cm^{-2} . The central wavelength of the laser was 778.6 nm, and the offset frequency was set to $f_{\text{off}} = 14.5 \text{ MHz}$. Several aspects of Fig. 2.2 are noteworthy. First, every line in the $5d$ spectrum has a corresponding line in the ion spectrum, and *vice versa*. That is, the ion signal has exactly the same information content as the photon signal. It should also be noted that the ion population is nearly an order of magnitude greater than the $5d$ population. This does not indicate that ionization is significantly depleting the atomic population. Rather, what it shows is that once an ion is formed it cannot relax back into a neutral state. Therefore, ions accumulate throughout the 950 pulse interrogation time. The $5d$ states, on the other hand, are constantly decaying and being re-excited. An estimate of the number of photons that are produced on the $6p \rightarrow 5s$ transition from cascade decays of the $5d$ states shows that an atom would emit, on average, about 5 photons at 420 nm during this interrogation time. Thus, the photon yield and ion yield are quite comparable for these typical laser intensities. However, the detection efficiencies for ions and photons can differ substantially.

One might expect additional structure in the ion spectra from 2-photon ionization of

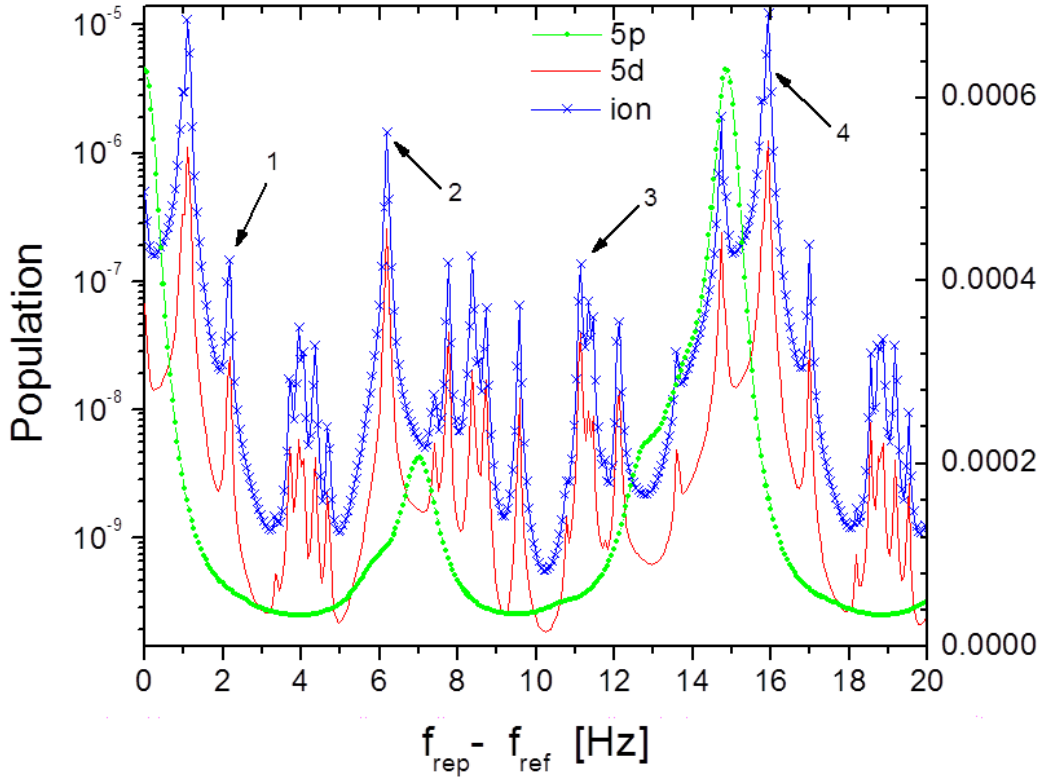


Figure 2.2: Plot of the relative populations in the 5p, 5d and Rb^+ manifolds as functions of the comb laser repetition frequency, minus a fixed reference frequency, $f_{\text{ref}} = 75557551$ Hz. The 5p population is plotted as round points connected by a line (green) and uses the linear scale on the far right; the 5d population is plotted as a solid line without points (red) and uses the log scale on the left; the Rb^+ population is plotted as crosses connected by a line (blue) and also uses the log scale on the left. All of the peaks in the 5d and ion curves have been identified as resulting from 2-photon transitions from the $5s \rightarrow 5d$ manifolds. A few selected peaks are labeled as (1) $5s_{1/2}, F = 1 \rightarrow 5d_{5/2}, F = 2$; (2) $5s_{1/2}, F = 2 \rightarrow 5d_{5/2}, F = 2$; (3) $5s_{1/2}, F = 1 \rightarrow 5d_{5/2}, F = 1$; (4) $5s_{1/2}, F = 2 \rightarrow 5d_{5/2}, F = 4$.

atoms in the $5p$ states. That is, once an atom has been excited to a $5p$ state, virtually *any* pair of comb teeth is “resonant” with 2-photon ionization to a continuum. This 2-photon process is similar to the one that excites states from the $5s$ to the $5d$ manifold, but should occur when a comb tooth has a frequency resonant with a $5s \rightarrow 5p$ transition. However, the ion signal shows no structure corresponding to direct $5p$ excitation, followed by 2-photon ionization.

To understand the reason for the lack of $5p$ structure in the ionization spectrum we tried to estimate the probability for direct 2-photon ionization of the $5p$ states. To do this we modified our code, prohibiting spontaneous emission from the $5p$ states. (Stimulated emission and absorption were still permitted.) We then artificially set the initial population of the $5p$ manifold to vary sinusoidally with f_{rep} , with its population shared equally between all states in the manifold. The remainder of the population was equally split between the 2 states in the $5s$ manifold. The result of this calculation is shown in Fig. 2.3, where we plot manifold populations as a function of f_{rep} . Clearly, the ion population follows the $5d$ population, even though the $5p$ population is many orders of magnitude larger than that of the $5d$ manifold. However, we can also see that the ion population does not have the detailed structure contained in the $5d$ spectrum, but rather has the smooth profiles of the $5p$ spectrum. Based on this calculation we estimate that, for the intensity used in these computations, the probability of 2-photon ionization from the $5p$ states is on the order of 10^{-5} . Recognizing that this analysis is crude, we nevertheless can say that for the realistic calculations typified by Fig. 2.2, when a comb tooth is resonant with a $5s \rightarrow 5p$ transition, the population of the $5p$ manifold is about 10^{-4} , and that the resulting 2-photon ionization should be on the scale of 10^{-9} , consistent with us not seeing it in the spectra.

2.4 Additional Results

A related question is why is the $5p$ population so small? The absence of nearly all direct $5p$ excitation from $5s$ is readily explained by optical pumping, which is the process whereby

light depletes a state in atoms and molecules by moving most of the electrons from this state to some other state. In Fig. 2.4 we plot the population of the $5p$ manifold as a function of $f_{rep} - f_{ref}$ for two different laser intensities. We see that the peak corresponding to the $5s_{1/2}, F = 2 \rightarrow 5p_{3/2}, F = 2$ transition disappears when the intensity of the laser is increased by a factor of 10. Further evidence of optical pumping is shown in Fig. 2.5a where we plot the $5s$ hyperfine levels $F = 1$ and $F = 2$ as a function of $f_{rep} - f_{ref}$. For the lower intensities, optical pumping is not noticeable, but by increasing the intensity by a factor of 10 almost all the population is pumped from $F = 2$ to $F = 1$ as shown in Fig. 2.5. Therefore, attempting to see the $5p$ population by increasing the laser intensity, results in increased optical pumping to an inaccessible $5s$ hyperfine level. The only two transitions in this system for which optical pumping does not take place are $5s_{1/2}, F = 2 \rightarrow 5p_{3/2}, F = 3$ and $5s_{1/2}, F = 1 \rightarrow 5p_{3/2}, F = 0$.

As Eq. 1.2 shows, the frequency of the n^{th} comb tooth depends on both f_{rep} and f_{off} . This means that it should be possible to have one comb tooth resonant with, say, the $5s_{1/2}, F = 2 \rightarrow 5p_{3/2}, F = 2$ transition, and a second tooth resonant with the $5s_{1/2}, F = 1 \rightarrow 5p_{3/2}, F = 2$ transition. In this case, much less optical pumping should take place.¹⁸ In Fig. 2.5c (low intensity) and Fig. 2.5d (high intensity) we plot the $5s_{1/2}$ hyperfine levels $F = 1$ and $F = 2$ as a function of $f_{rep} - f_{ref}$, but now with a value of f_{off} chosen to negate optical pumping. The contrast between plots 2.5b and 2.5d is obvious.

Next we decided to see what the effect of a quadratic spectral phase $\varphi(\omega) = C\omega^2$ (where C is the chirp parameter) has on excitation. In this calculation instead of varying the repetition frequency of the laser we decided to take two peaks from Fig. 2.2, one at 18.72 Hz and the second at 6.18 Hz and watch the populations of the states as we varied the chirp parameter. The peak values of these two transitions are shown in Fig. 2.6, plotted versus the chirp parameter. The first transition is called a type A transition by Felinto¹⁵ and is the result of two photon excitation via a resonant transition to an intermediate state. The second transition (type B) is the result of two photon excitation via a non-resonant

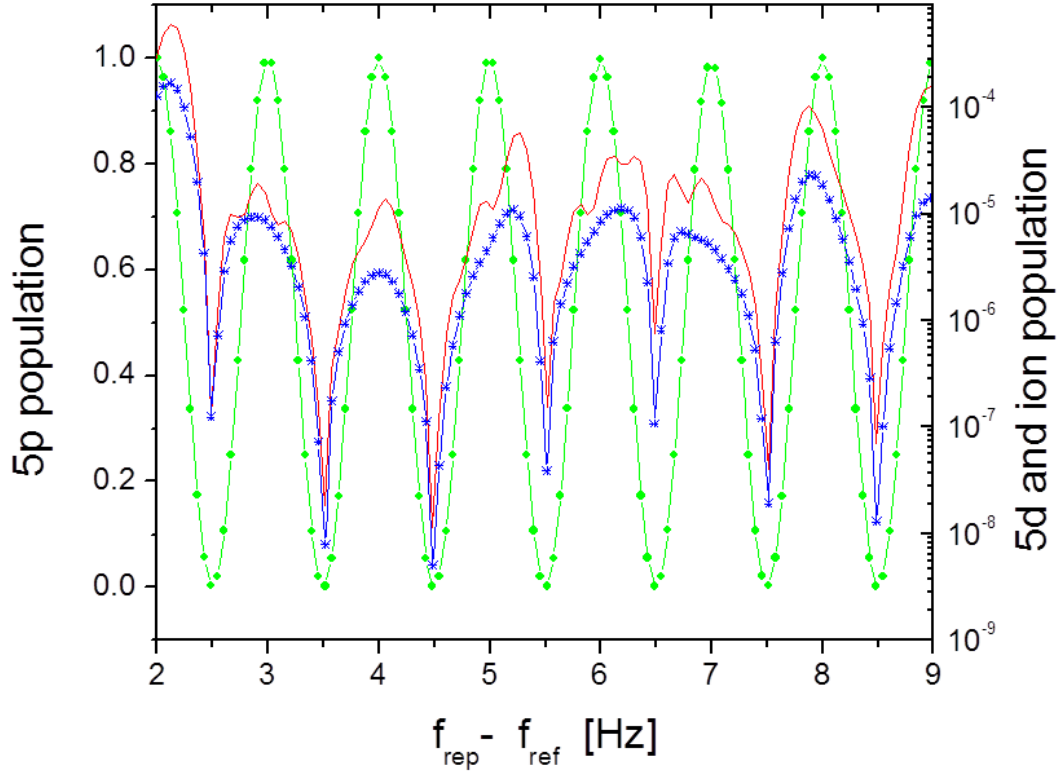


Figure 2.3: *Computation of 5d (solid line without points, red) and ionization (solid line with crosses, blue) manifolds under the artificial initial condition that the initial population of 5p states (solid line with circular points, green) varies sinusoidally with f_{rep} . The ionization population largely follows the 5d population. However, the lack of 5d structure in the ionization population is an indication of 2-photon ionization of states in the 5p manifold (without being resonant with an intermediate 5d state.)*

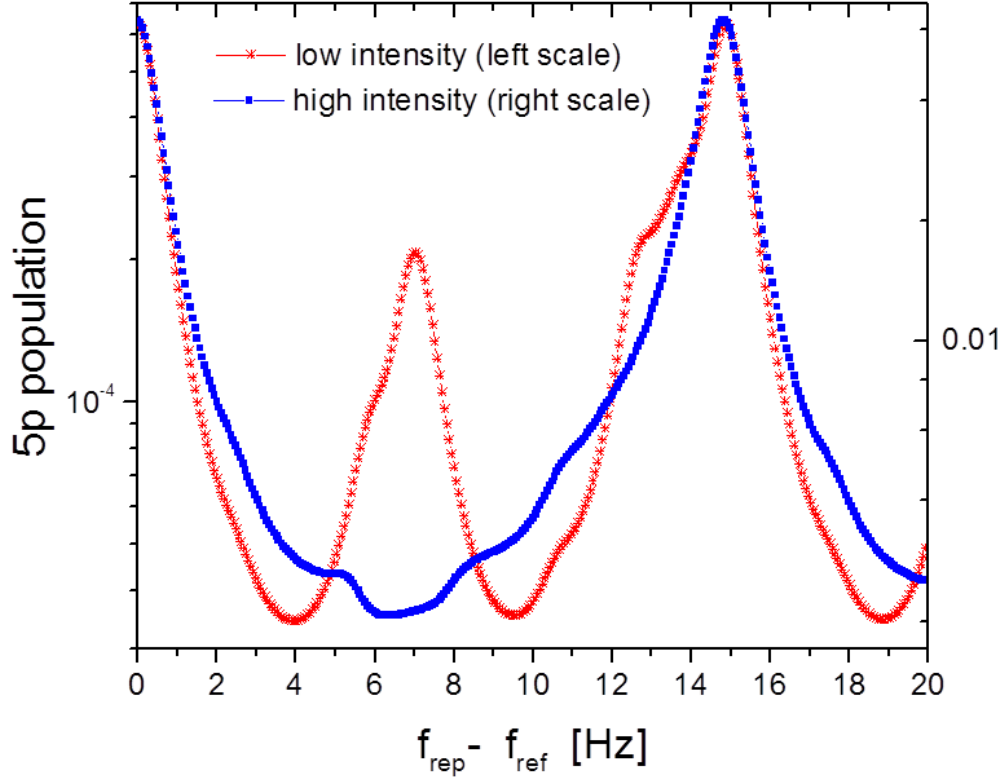


Figure 2.4: *Detail of 5p population for low and high intensity comb laser. The peak near 7 Hz is from the $5s_{1/2}, F = 2 \rightarrow 5p_{3/2}, F = 2$ transition and clearly shows the effects of optical pumping. The peak near 15 Hz is from the $5s_{1/2}, F = 2 \rightarrow 5p_{3/2}, F = 3$ transition, for which no optical pumping is expected. The two curves were scaled such that the peaks near 15 Hz had the same magnitude.*

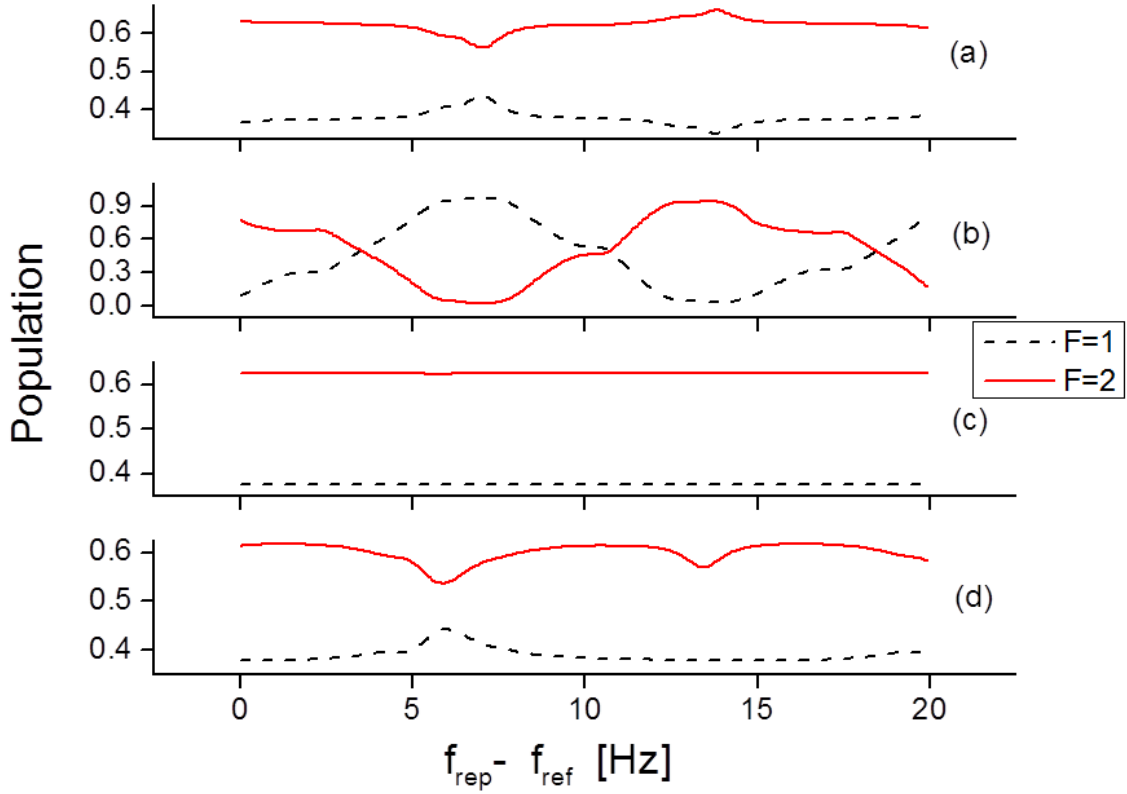


Figure 2.5: Ground state hyperfine populations versus f_{rep} when a comb tooth is resonant with the $5s_{1/2}, F = 2 \rightarrow 5p_{3/2}, F = 2$ transition. (a) is for low comb laser intensity and does not exhibit strong optical pumping. In (b) the comb laser intensity is high and strong optical pumping from $5s_{1/2}, F = 2$ to $5s_{1/2}, F = 1$ is clearly seen. (c) and (d) are the same intensity conditions as (a) and (b), respectively, but f_{off} has been adjusted such that a second comb tooth is resonant with the $5s_{1/2}, F = 2 \rightarrow 5p_{3/2}, F = 2$ transition. The optical pumping is minimal, as expected.

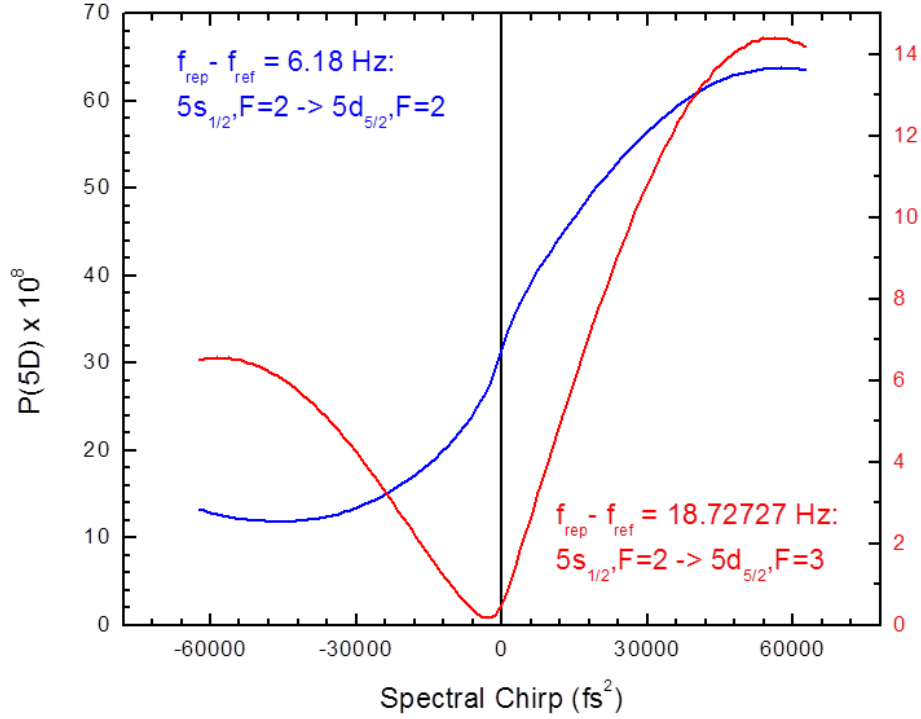


Figure 2.6: This is a plot of two particular states' populations as a function of chirp parameter. The blue curve on the graph is a so-called Type A transition (see text for details) and the red curve is a Type B transition.

transition to an intermediate state. Similar calculations were made by Felinto but only with two values of chirp parameter. In Fig. 2.6 we present results of our calculation with a large range of chirp parameters.

From Fig. 2.6 we see huge effects in excitation signal when pulses are chirped. From Felinto,¹⁵ this enhancement can be explained using 2nd order perturbation theory.¹⁹

$$a \approx \frac{-1}{i\hbar^2} \mu_{fi} \mu_{ig} \left[i\pi E(\omega_{ig}) E(\omega_{fg} - \omega_{ig}) + \wp \int_{-\infty}^{+\infty} \frac{E(\omega) E(\omega_{fg} - \omega)}{\omega_{ig} - \omega} d\omega \right] \quad (2.3)$$

where a is the excitation amplitude, μ is the dipole matrix element, E is the electric field

of the laser pulses, the subscripts ig and fg refer to transitions between the ground to intermediate and ground to final states, respectively, the integral is over all frequencies in the optical spectrum, and now E includes the phase term containing the chirp parameter. Note that a positive value of C means that the frequencies contained in the pulse are time-ordered from low to high, and a negative value of C means the frequencies are ordered from high to low. In this equation the two terms in the brackets represent resonant (first term) and off-resonant (second term) excitation contributions, and they are shifted by $\pi/2$ with respect to each other. Furthermore, the off-resonant term is asymmetric about the resonance frequency, which results in a π phase difference between the blue and red portions of the spectrum. Type A transitions can be understood very easily with this model. For this transition we only have the first term in Eq. 2.3. In Rb atoms $5s - 5p$ transitions correspond to 780 nm and $5p - 5d$ transitions correspond to 776 nm. In the case of negative chirp, 776 nm photons interact with the target system first and 780 nm photons later, which means that a $5p - 5d$ transition would have to happen first and $5s - 5p$ second, which automatically lowers the excitation amplitude. However, for a positive chirp, the $5s - 5d$ transition would be driven first, which leads to a much larger excitation amplitude.

As for the Type B transitions, the second term in the Eq. 2.3 becomes dominant over the first one. When the pulse is transform-limited (for which case the chirp parameter is 0), the transition amplitude is zero because the symmetric composition of the red and blue components in the spectrum gives rise to an anti-symmetric integrand. But any little phase (either positive or negative) added to the spectrum results in breaking the anti-symmetry and correspondingly gives rise to a greater excitation amplitude. It is also noticeable from Fig. 2.6 that a positive chirp enhances the transition much more compared to a negative chirp and the reason for this is the same as for the Type A transitions.

Last, we varied the number of pulses in the train. Computation time is linear in the number of pulses in the train; if we can decrease the number of pulses in the train without significantly affecting the spectra, then the computations can be done more readily. However,

as the number of pulses decreases, the width of the comb teeth grows, leading to a broadening of the structure in our spectra.¹⁵ Furthermore, as already demonstrated,¹⁵ fewer pulses in the train means less overall population movement. Figure 2.7 shows the same calculation as in Fig. 2.2 but with 50 pulses in the train. One can see that the structure is broader and the excitation/ionization decreased, as expected. However Fig. 2.7 still reflects the essential features of the Rb atom’s structure, but with about 5% of the computer time (a couple of hours on our system). In passing, we note that the $5d$ spectrum, for example, has additional “ringing” on it compared to the corresponding spectrum in Fig. 2.2. The ringing exists because the Fourier transform of a finite pulse train is the convolution of the Fourier transform of an infinite train (an ideal comb) with the Fourier transform of a square pulse having temporal width equal to the number of pulses in the train divided by f_{rep} . The ripples, then, are actually a sinc function on the comb teeth and are reflected in the excitation spectra.

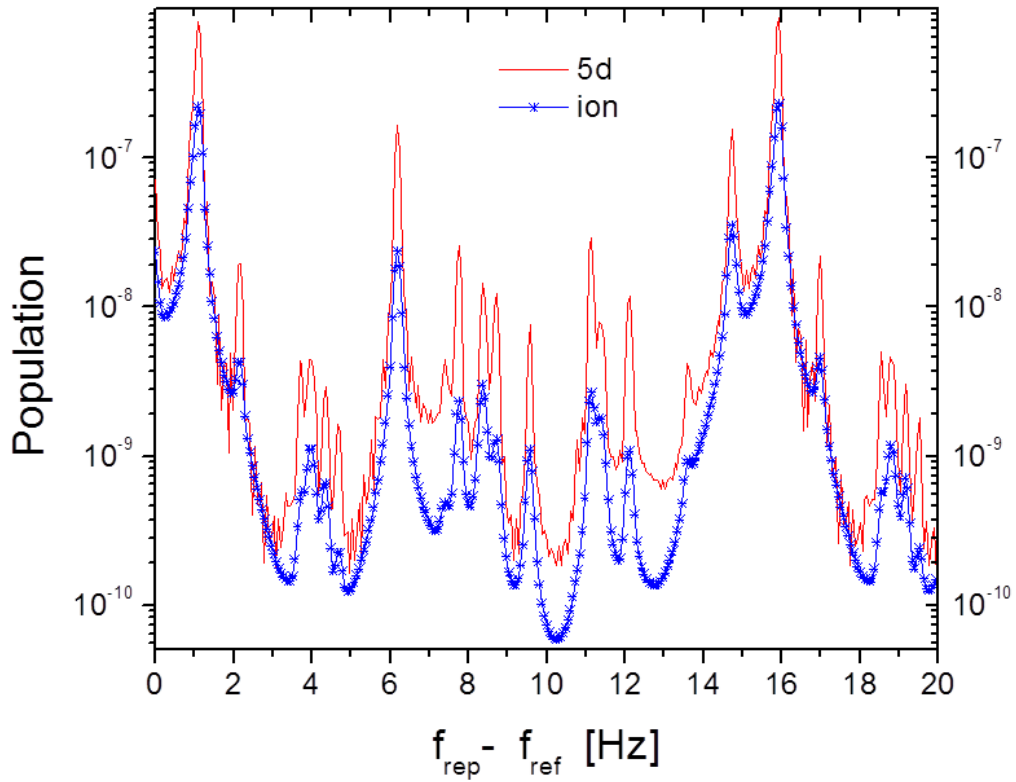


Figure 2.7: *The same as Fig. 2.2, but for 50 pulses in the train. The peaks are slightly broader and “ringing” is seen in the populations. The ringing is real, and is actually due to the Fourier transform of a rectangular pulse, superimposing a sinc function on the comb teeth, and is especially evident on the 5d curve.*

Chapter 3

Experimental Setup

It seems that our newly developed theory shows and predicts lots of very interesting results. So we decided to go to the lab, set up the experiment and test these results. In this chapter the experimental setup that was used to test our newly developed theoretical model is described.

An overview of the chapter is as follows: First we talk about our target system and how we cool and trap it. In the following subsection we also describe how we lock the lasers necessary to cool and trap the neutral Rb atoms. Then, the next section describes the detection of the ions that were produced by the frequency comb. In the third section the experimental scheme itself for doing DFCS with ion detection is described. The last section discusses the data acquisition system.

3.1 Target System

Doing spectroscopic measurements of a target system requires a lot of things to be taken care of, such as Doppler broadening effects, power broadening,²⁰ reducing background counts and reducing the errors in the experiment. Even though our goal was just to see whether the ionization is negligible or not in DFCS and we were not concerned much with a very high precision measurement, we still tried to reduce some experimental uncertainties that would make our measurements unreliable. One of the biggest uncertainties in any experimental measurement comes from the Doppler broadening effect which is the result of the target

system having a significantly wide range of translational velocities. In our experiment we reduce this broadening effect by cooling and trapping our target. Cooling just simply means slowing down the target system, and trapping is localizing the cloud of the cold target. Cooling and trapping of neutral atoms have been documented in many research articles²¹⁻²³ so here I will just briefly mention the main principle of the processes.

The best candidates to cool and trap are alkali metal atoms, because of the fact that they have one unpaired electron in the outer s shell and excitation of that electron is used for the cooling cycling transition. For our experiment we decided to cool and trap ^{87}Rb atoms since they have relatively simple structure. This was done by a Magneto Optical Trap (MOT) setup. As is documented in many articles²¹⁻²³ cooling and trapping of target atoms in a MOT is done by combination of laser light and a spatially dependent magnetic field. The laser light acts as a source of so-called radiation pressure force that, by interacting with the atoms, slows them down. As for the magnetic field, it causes Zeeman splitting of the target atoms and the force becomes position dependent with respect to the magnetic field; this causes trapping at the zero of the magnetic field. A simplified energy level diagram for the MOT transitions in ^{87}Rb is given in Fig. 3.1.

On the same graph we show the trapping laser transition as well. The laser is actually detuned from resonance; this is required to slow down the atoms in a MOT.²¹⁻²³

But having only a trapping laser is not sufficient for cooling and trapping. The reason is that the trapping laser, in addition to exciting the target atom from $5s_{1/2}, F = 2$ to $5p_{3/2}, F = 3$, sometimes excites the system from $5s_{1/2}, F = 2$ to $5p_{3/2}, F = 2$. Once the system is in this state it has two states in the $5s_{1/2}$ manifold to decay to: $F = 1$ or $F = 2$. But the $F = 1$ state acts like a dark state since the trapping laser is not resonant with any transition out of that state. The probability of exciting the system from $5s_{1/2}, F = 2$ to $5p_{3/2}, F = 2$ with the trapping laser is about 0.1 %. This seems to be very small but over many optical cycles (roughly a millisecond for Rb) all the atoms end up in the $5s_{1/2}, F = 1$ state and fall out of the MOT. That is why a second laser, called the repump laser, is used.

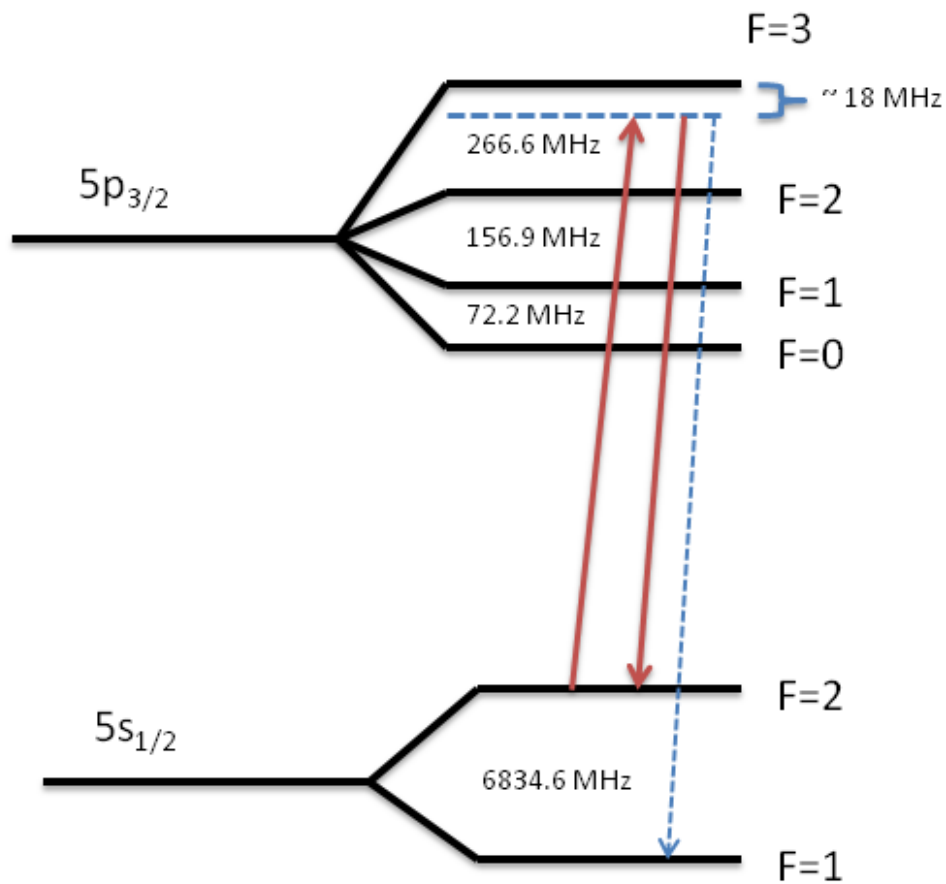


Figure 3.1: *Hyperfine structure of $5s_{1/2}$ and $5p_{3/2}$ states of Rb atoms. The solid red arrow pointing up shows trapping transition red detuned from resonance. The solid red arrow pointing down and the dashed blue arrow show the decay possibilities.*

The laser is resonant with the $5s_{1/2}, F = 1$ to $5p_{3/2}, F = 2$ transition and puts the “stray” atoms back into the cycle. A schematic of the repumping transition is given in Fig. 3.2.

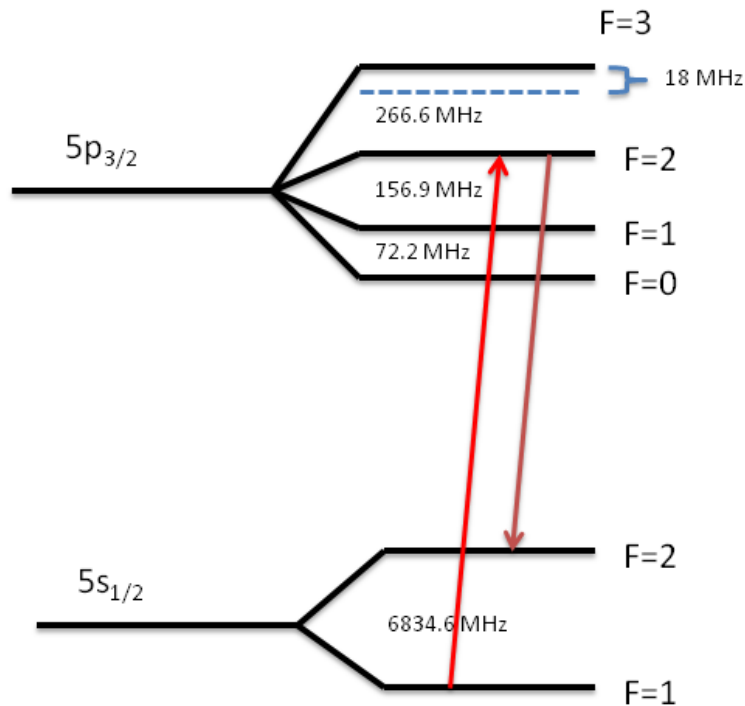


Figure 3.2: *Hyperfine structure of $5s_{1/2}$ and $5p_{3/2}$ states of Rb atoms. Solid red arrow pointing up shows repump transition.*

With this MOT setup we cooled our target to 120 micro-Kelvin, which allowed us to neglect the Doppler broadening effect. The density of our cooled and trapped atoms was 10^{10} cm^{-3} and was confined to a roughly spherical volume having a diameter of a couple of millimeters.

3.1.1 Laser locking

In order to obtain and maintain a stable MOT, the stability of both trapping and repump lasers is crucial. This means that the laser frequencies need to be stabilized with very stable frequency references. In our case the lasers were locked to Rb atom hyperfine transitions. This was accomplished using a Rb saturated absorption setup and a very robust “peak locking”²⁴⁻²⁷ scheme. A schematic for the saturated absorption setup that was used to lock the repump laser is shown in Fig. 3.3.

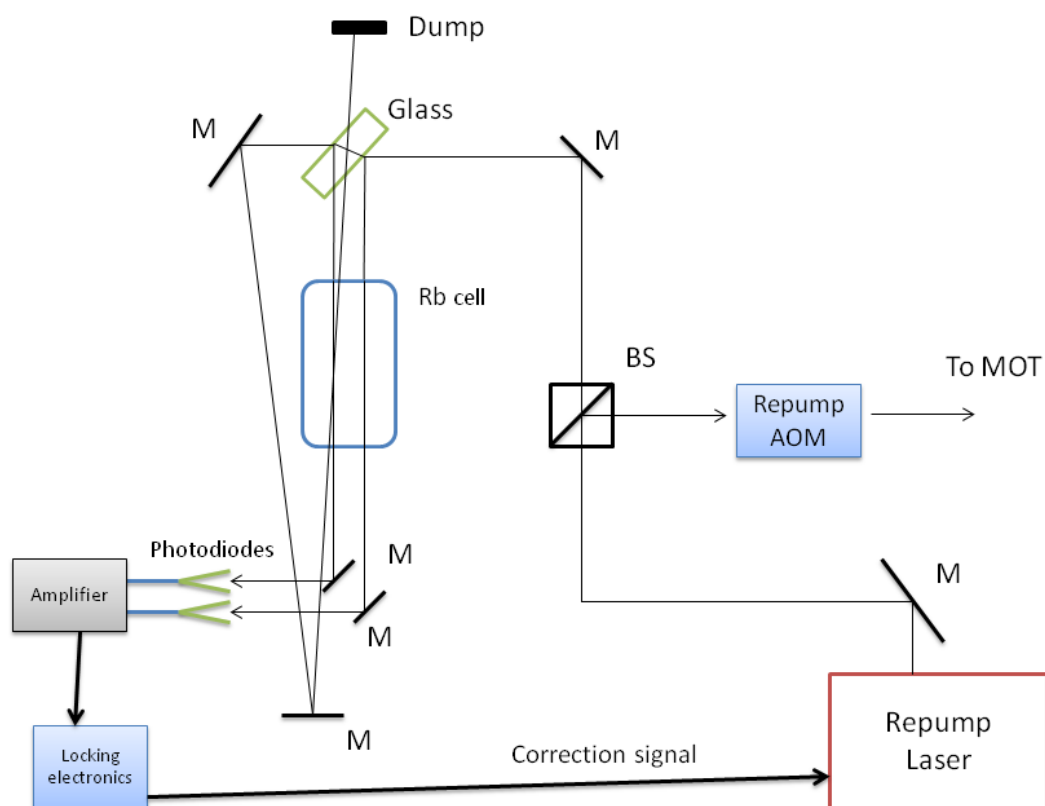


Figure 3.3: Schematic of saturated absorption setup for the repump laser; M-Mirror, BS-Beam Splitter.

At first it seems strange that we can use an absorption signal from a room temperature Rb cell to lock our lasers with Doppler-free precision. However, we employ a saturated

absorption scheme that uses two counter-propagating beams, one of which is strong (the so-called pump beam) and the other of which is weak (the so-called probe beam). This scheme gives us a Doppler-free spectrum to which we can lock our lasers.²⁵

The repump laser was locked to the so-called 1-2 crossover peak²⁸ which is halfway between $5s_{1/2}, F = 1 - 5p_{3/2}, F = 1$ and $5s_{1/2}, F = 1 - 5p_{3/2}, F = 2$. This is schematically shown in Fig. 3.4. This signal is the strongest compared to other peaks in the saturated absorption spectrum and that made the locking more robust. But before going into the MOT the laser frequency was changed to the correct frequency necessary for the MOT repump transition using an Acousto Optical Modulator (AOM).

For locking the repump laser, a laser frequency dither method was used. This means that the laser frequency was repeatedly swept back and forth through the resonance, allowing electronics to lock the laser to the peak in the saturated absorption spectrum.²⁴ This method has the drawback of effectively broadening the laser bandwidth. However for a re-pump laser, this was not a problem.

Since a narrow bandwidth for the trapping laser is more crucial in constructing a MOT than a narrow bandwidth for the repump laser, a magnetic field dither method was used for its locking.²⁴ In Fig. 3.5 we show the saturated absorption setup for the trapping laser. This setup is very similar to the one for the repump laser. The only difference is that the Rb cell is inside a Zeeman solenoid, and instead of linearly polarized light, circularly polarized light was used. In a Zeeman dither lock, instead of sweeping the laser through the transition resonance, the resonance itself is swept back and forth using the Zeeman effect.

The trapping laser was locked to the so-called 2-3 crossover peak shown in Fig. 3.4. Then using an AOM, it was upshifted to the correct trapping frequency, before going into the MOT chamber.

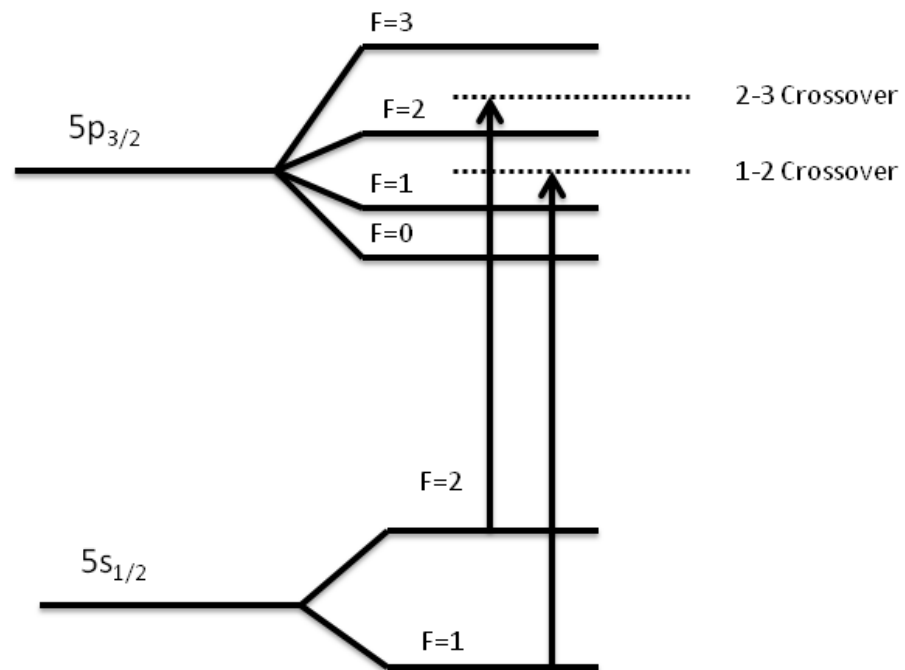


Figure 3.4: *Hyperfine structure of Rb $5s_{1/2}$ and $5p_{3/2}$ including (1-2) and (2-3) crossover “states”.*

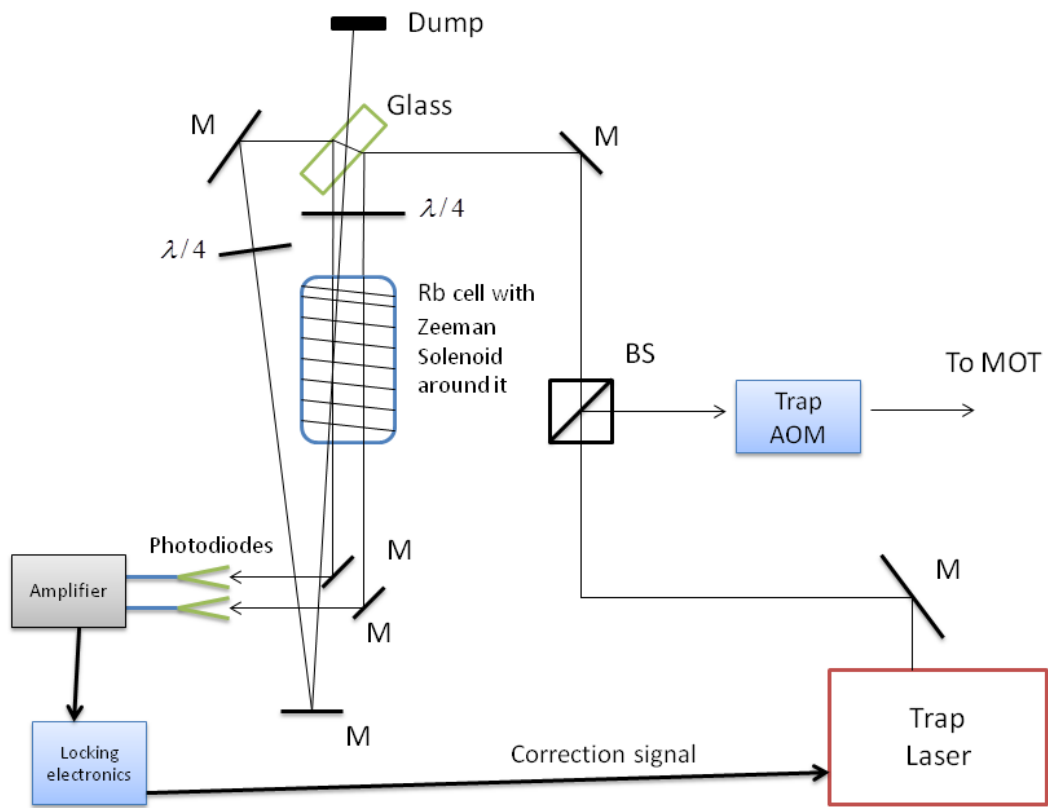


Figure 3.5: Schematic of saturated absorption setup for the trapping laser; *M*-Mirror, *BS*-Beam Splitter, $\lambda/4$ (quarter) wave plate.

3.2 Ion Detection

As was mentioned in the introduction the goal of this research was to count the ions that were produced in a cold target by a frequency comb. Our experimental setup is able to do so because inside the trapping region a Recoil Ion Momentum Spectrometer (RIMS)^{29,30} is built. A schematic of this arrangement is shown in Fig. 3.6.

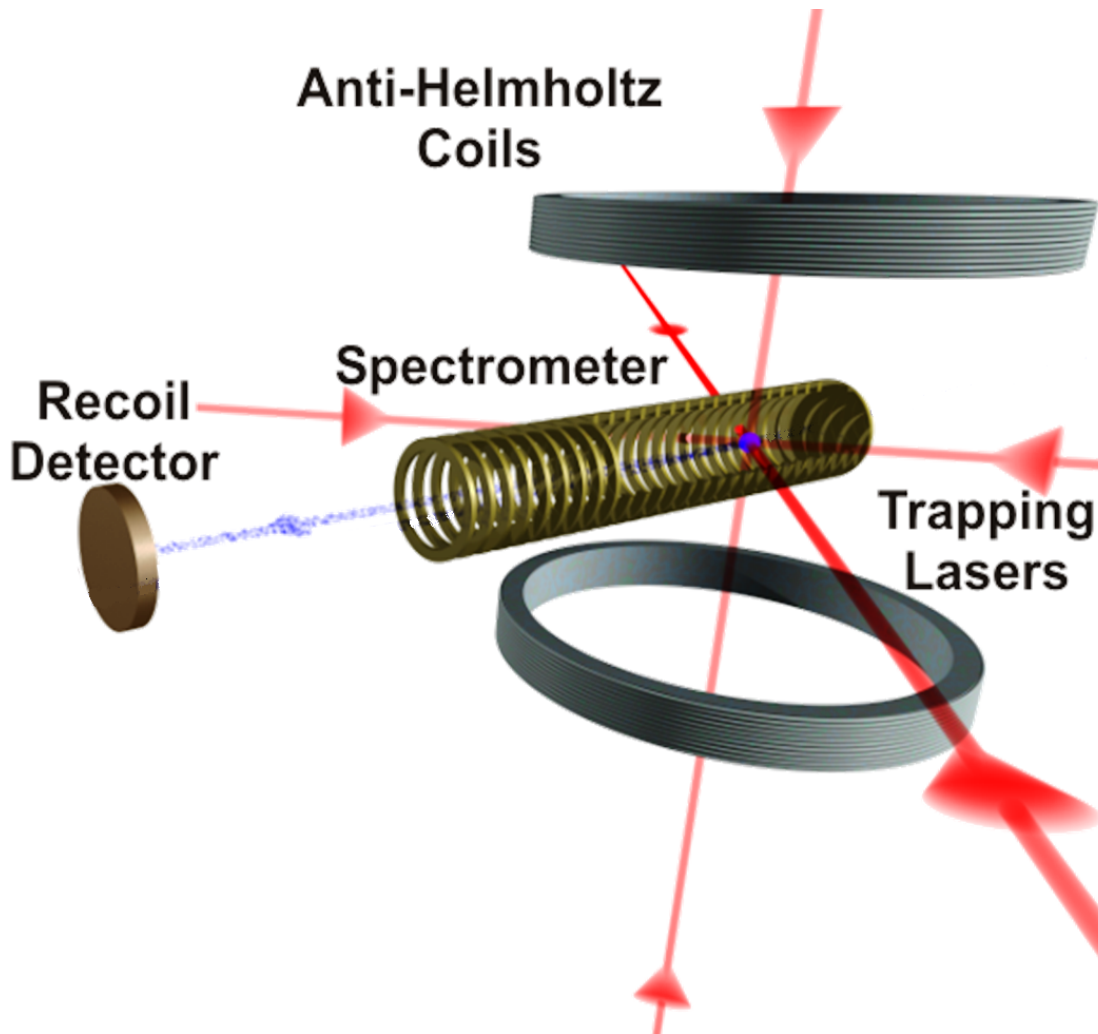


Figure 3.6: Recoil Ion Momentum Spectrometer used for collecting the ions. Anti-Helmholtz coils are for the MOT. Ions produced inside the trapping chamber are extracted with the electric field applied on the spectrometer and directed onto a recoil ion detector.

Any ions that were produced inside the chamber were extracted with the electric field

applied on the spectrometer and directed toward the 2D position sensitive detector. The value of the electric field is 10 V/cm . Because the field is so small we can neglect the Stark shift of the Rb atom energy levels.

3.3 Experimental Setup for DFCS

A simplified schematic for an oscillator that is used to generate a frequency comb is shown in Fig. 3.7. It consists of a crystal, dispersion compensation prisms, an output coupler, and

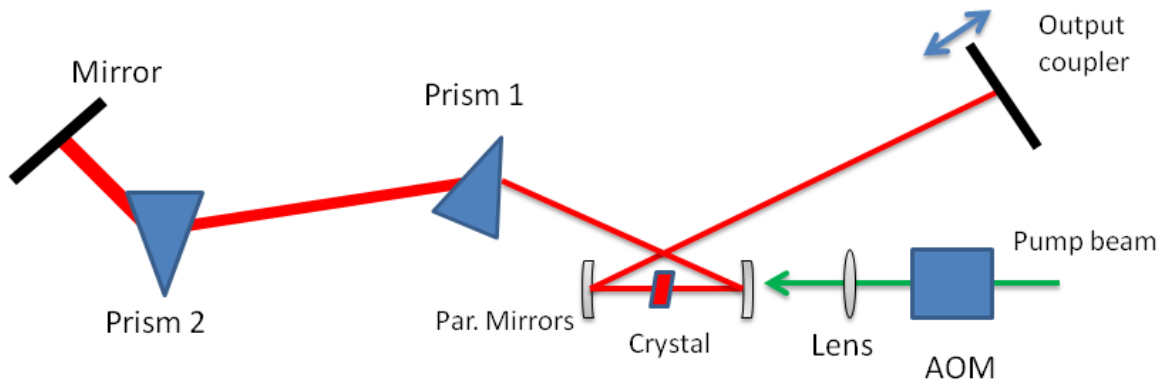


Figure 3.7: *Simplified schematic of an oscillator. It consists of a couple of prisms, a crystal, an output coupler and a pump laser.*

a pump laser.

Doing DFCS, as was explained in the introduction, requires simultaneous control over f_{rep} and f_{off} . In general, changing and controlling f_{rep} is done by moving the output coupler which causes the cavity length, and hence the time between laser pulses, to change. Controlling f_{off} is done by modulating the pump power going into the crystal. To see how this works it is better to look at the expression for the offset frequency:

$$f_{\text{off}} = f_{\text{rep}}(2\pi\varphi_{\text{cep}})^{-1}, \quad (3.1)$$

where φ_{cep} is the carrier envelope phase, which is proportional to the difference between the inverses of the group and phase velocities. Modulating the pump power causes temperature of the crystal to change which results in a crystal length change, and hence it adds this phase shift.

But unfortunately not all oscillators have individual control over f_{rep} and f_{off} . Our Kansas Laser Source KLS oscillator is one of those. In our lab we are only able to control the ratio between f_{rep} and f_{off} which means that our oscillator has CEP locking capability, but we cannot lock and vary f_{rep} and f_{off} individually. This is acceptable for the CEP dependent experiments that many in the Macdonald Lab do, but as far as DFCS experiment requirements go, it is not.

However with the existing oscillator we still managed to do the DFCS experiment but in a little bit different way. Instead of varying f_{rep} and f_{off} and counting the ions we decided to measure f_{rep} and f_{off} and do the experiment the other way around. I will discuss this a little bit later. In the next subsection I would like to talk very briefly how these f_{rep} and f_{off} measurements were done.

3.3.1 Measuring f_{rep} and f_{off}

The schematic for measuring f_{rep} and f_{off} is shown in Fig. 3.8. The output of our oscillator is split in two equal-intensity beams (50/50 splitter). The output then has 10 % split off

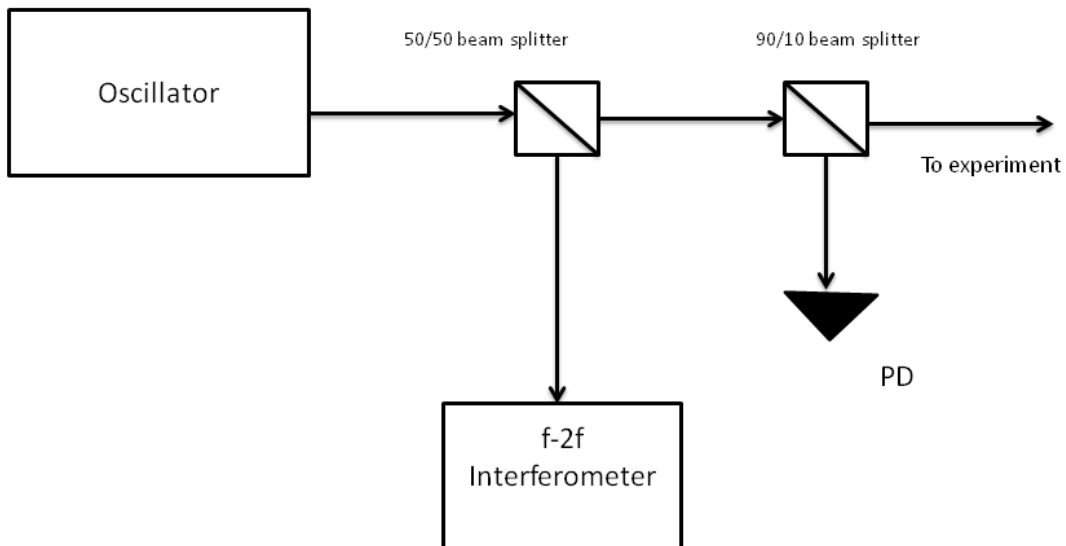


Figure 3.8: Schematic for measuring f_{rep} and f_{off} . Pulses coming from the oscillator are split in half with a 50/50 beam splitter; half goes to f - $2f$ interferometer and half goes to another beam splitter, 10% of which is used to read f_{rep} and the rest is sent to the MOT chamber.

and sent to a fast photodiode for the f_{rep} measurement. The remaining 90 % was used in the experiment. As for the second half, it was sent to the f-2f interferometer^{31,32} for measuring f_{off} . A schematic for the f-2f interferometer is shown in Fig. 3.9. It consists of a Photonic Crystal Fiber (PCF),³³ a dichroic beam splitter, a delay stage, a BBO crystal, a diffraction grating, an iris, an assortment of optics, and a detector. The PCF is responsible for generating an “octave in the spectrum”. That is, the output of the PCF stretches the frequency output of the laser to span an octave. This process is based on the so-called the Kerr effect.³⁴ Spectra of the pulses before and after our PCF are shown in Fig. 3.10.

As we see from the graph, the spectrum after the PCF covers an octave as it has wavelengths 532 nm through 1064 nm. This optically broadened pulse is then split using a dichroic beam splitter. The lower frequency components were transmitted and the higher ones were reflected. The lower frequency components were frequency doubled using a BBO crystal. The higher frequency components were sent to a delay stage and later combined with the frequency doubled component. The beat frequency (difference frequency) between the components is the offset frequency and it was measured using an avalanche photo-diode. The idea behind measuring the beat frequency is demonstrated schematically in Fig. 3.11. To accurately measure both f_{rep} and f_{off} signals, the photodiode outputs were referenced to the Global Positioning System (GPS).

3.3.2 Our experimental scheme

Now let’s return to our experimental setup. As we said earlier, our oscillator had no individual control over f_{rep} and f_{off} , so this is how we decided to do the DFCS experiment shown schematically in Fig. 3.12.

We took our KLS oscillator and didn’t lock either f_{rep} and f_{off} , or their ratio. In other words we used a free running oscillator and let nature help us to do this experiment, which basically means that the change in f_{rep} and f_{off} was done by the temperature fluctuations in the laser room. The pulses from the oscillator were directed to the MOT and the ionizations

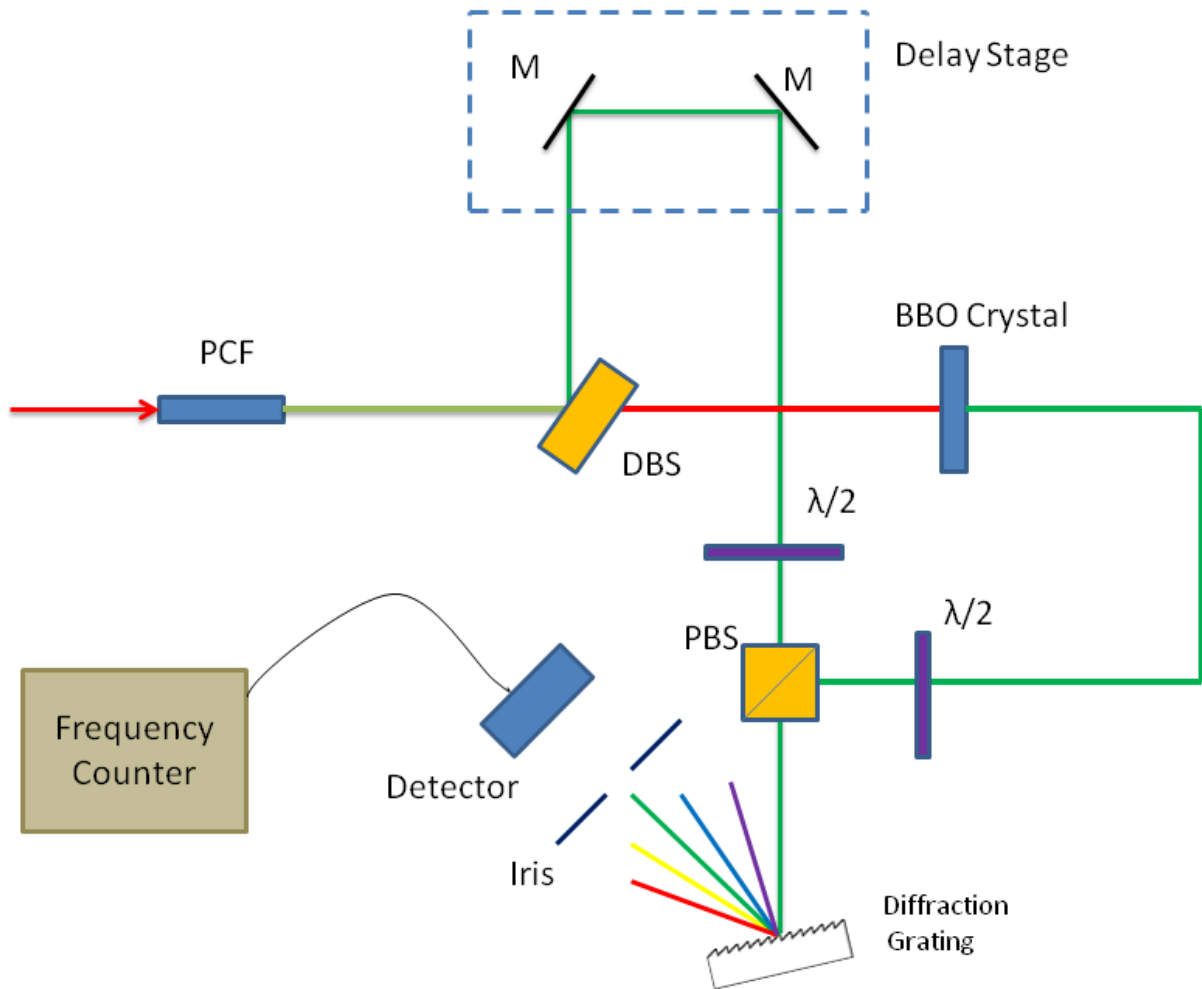


Figure 3.9: Schematic of an f - $2f$ interferometer; PCF-Photonic Crystal Fiber, DBS-Dichroic Beam Splitter, PBS- Polarized Beam Splitter. Pulses from the oscillator are sent through the PCF. It generates an octave in the laser spectrum. Then using the DBS, the pulses are split. The lower frequency components are transmitted and frequency doubled using a BBO crystal. The higher frequency components are reflected and sent to the delay stage. Later on these two arms are combined and a beat frequency is measured.

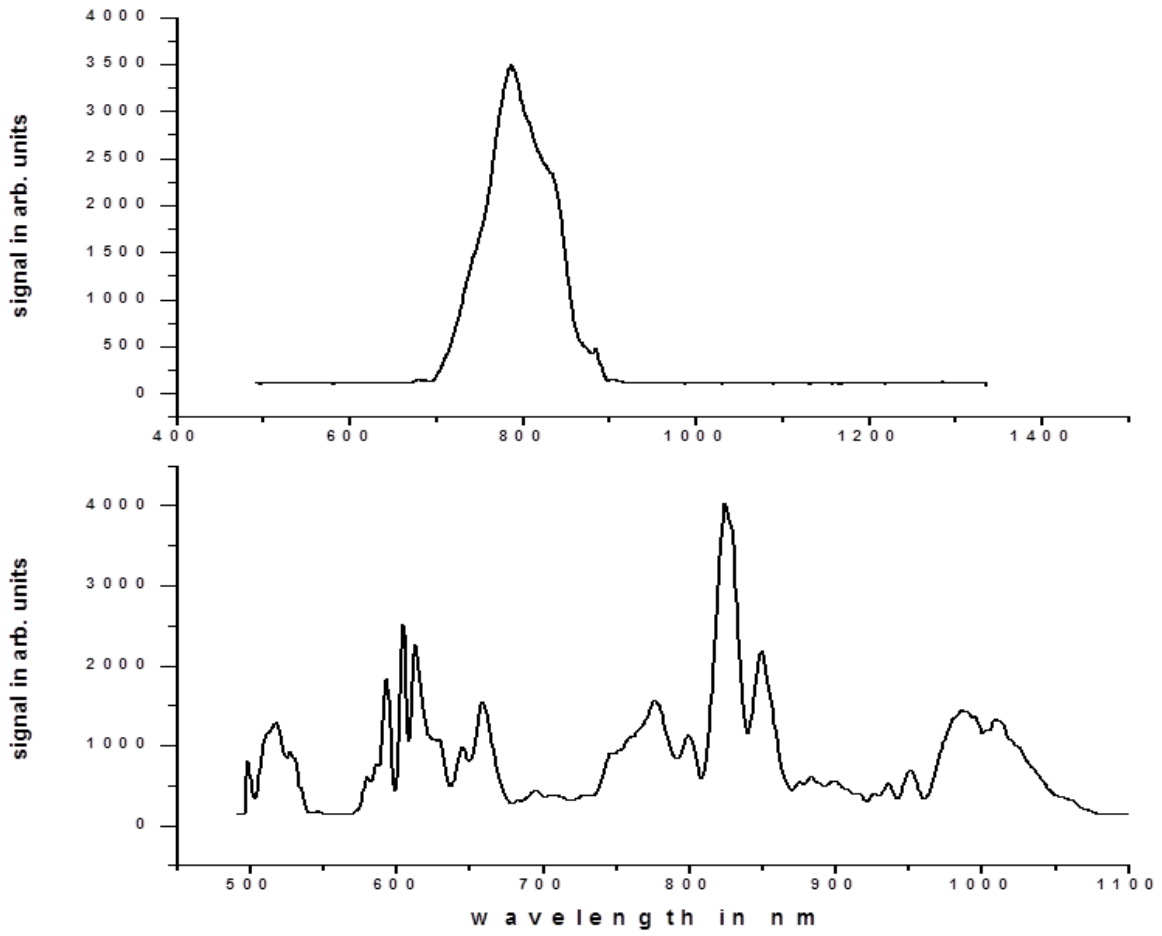


Figure 3.10: Spectra of the pulses before (top) and after (bottom) the PC Fiber. The lower spectrum covers an octave as it has 532 and 1064 nm photons in it.

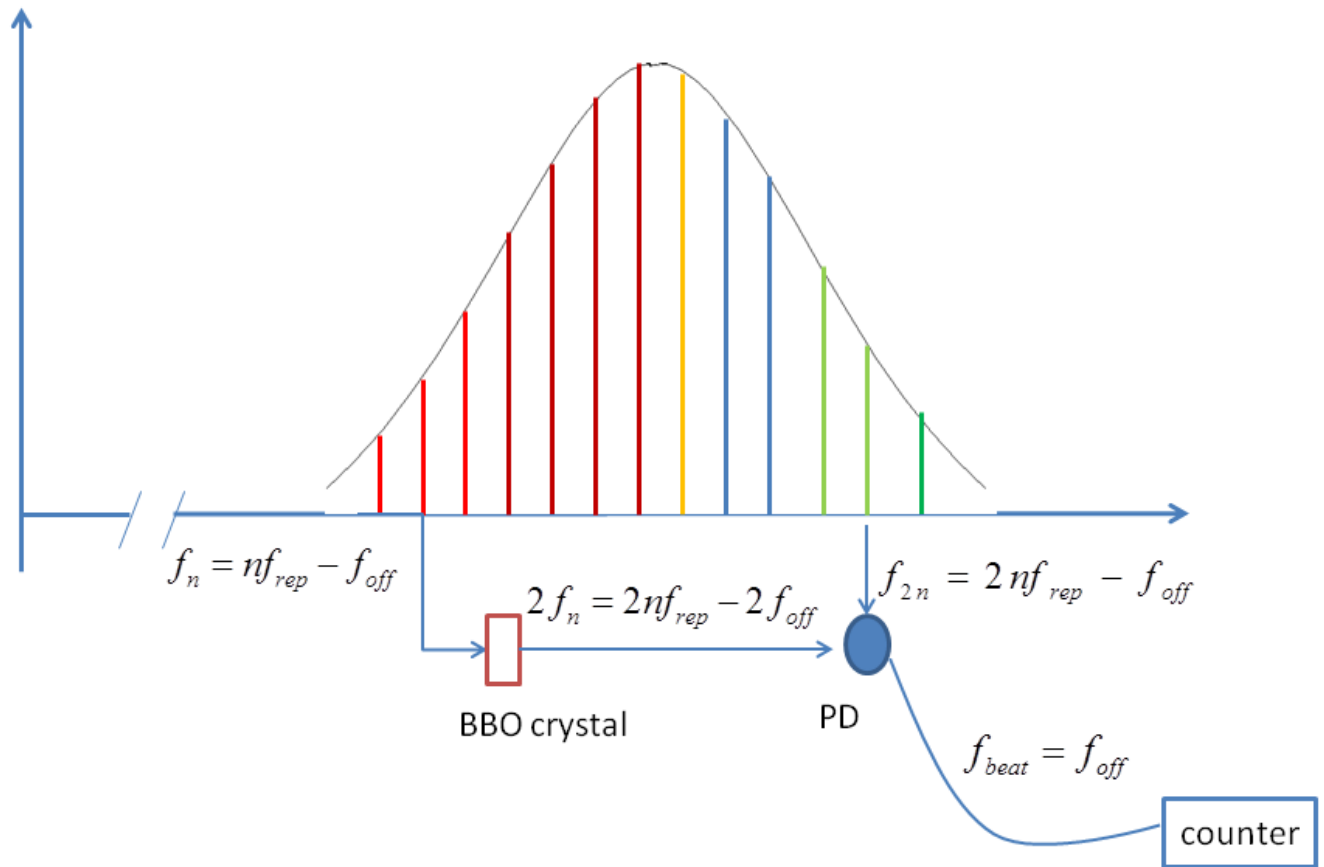


Figure 3.11: Idea behind the f - $2f$ interferometer. The spectrum shown above covers an octave as it has frequencies f_n and f_{2n} . Using a BBO crystal, the f_n component is frequency doubled and beat against f_{2n} . The beat frequency is the difference between the components and as is shown above, it is f_{off} .

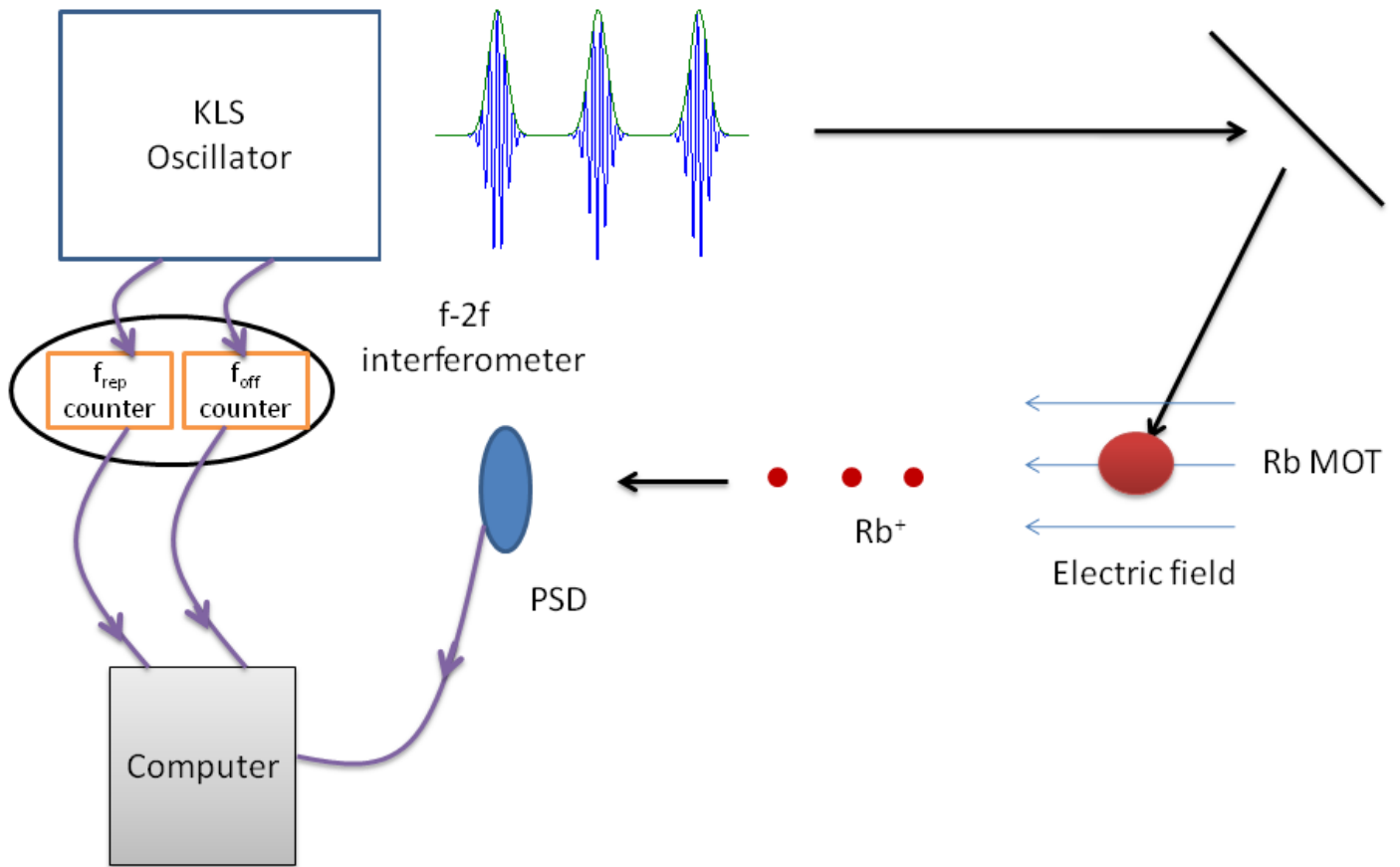


Figure 3.12: *Experimental scheme for DFCS. The pulses from the oscillator were sent to the MOT and the ions produced inside the chamber were counted simultaneously with f_{rep} and f_{off} .*

in the vapor were detected through the collection of ions on a PSD. I would like to emphasize that the PSD was mainly used as a typical ion detector since we were not interested with the position information of the ions. Meanwhile the parameters of the frequency comb, f_{rep} and f_{off} , that caused the excitation and the ionization, were measured. The gate time for this measurement was chosen to be 100 ms, which is the time necessary for the frequency counters to read f_{rep} and f_{off} with 0.1 Hz precision. The idea of the measurement is the following: In each 100 ms interval we read three numbers: the ions produced in the MOT, f_{rep} and f_{off} . In this measurement we were assuming that within 100 ms f_{rep} and f_{off} were not changing significantly, so our target was exposed to a real comb for 100 ms. As the temperature in the room changed, it caused f_{rep} and f_{off} to change and hence the ion signal to change as the comb teeth matched atomic resonances. For good statistics we ran our experiment for a couple of hours for each spectrum.

3.3.3 Stability of the laser and range of f_{rep} and f_{off}

Doing the experimental method just described above has some potential problems. First of all, to study the structure of Rb atoms some range of f_{rep} and f_{off} is necessary, so is the temperature fluctuation in the room enough? In the other words, is it going to cause enough change in f_{rep} and f_{off} to look at all the transitions in the atom? And second, is the laser stable in the 100 ms time interval, allowing us to assume that our target is exposed to a real comb?

To address the first issue we did the experiment shown schematically in Fig. 3.13. This is basically the same experimental scheme as our actual experimental one except that here we were not counting the ions. We took the output of our oscillator and split it in half. One part was directed onto a fast photodiode that was connected to a frequency counter, and the second we sent through the f-2f interferometer,^{31,32} the output of which was connected to a second frequency counter. These counters were reading the frequencies every 100 ms and these readings were stored in a computer. The result of this experiment is shown in

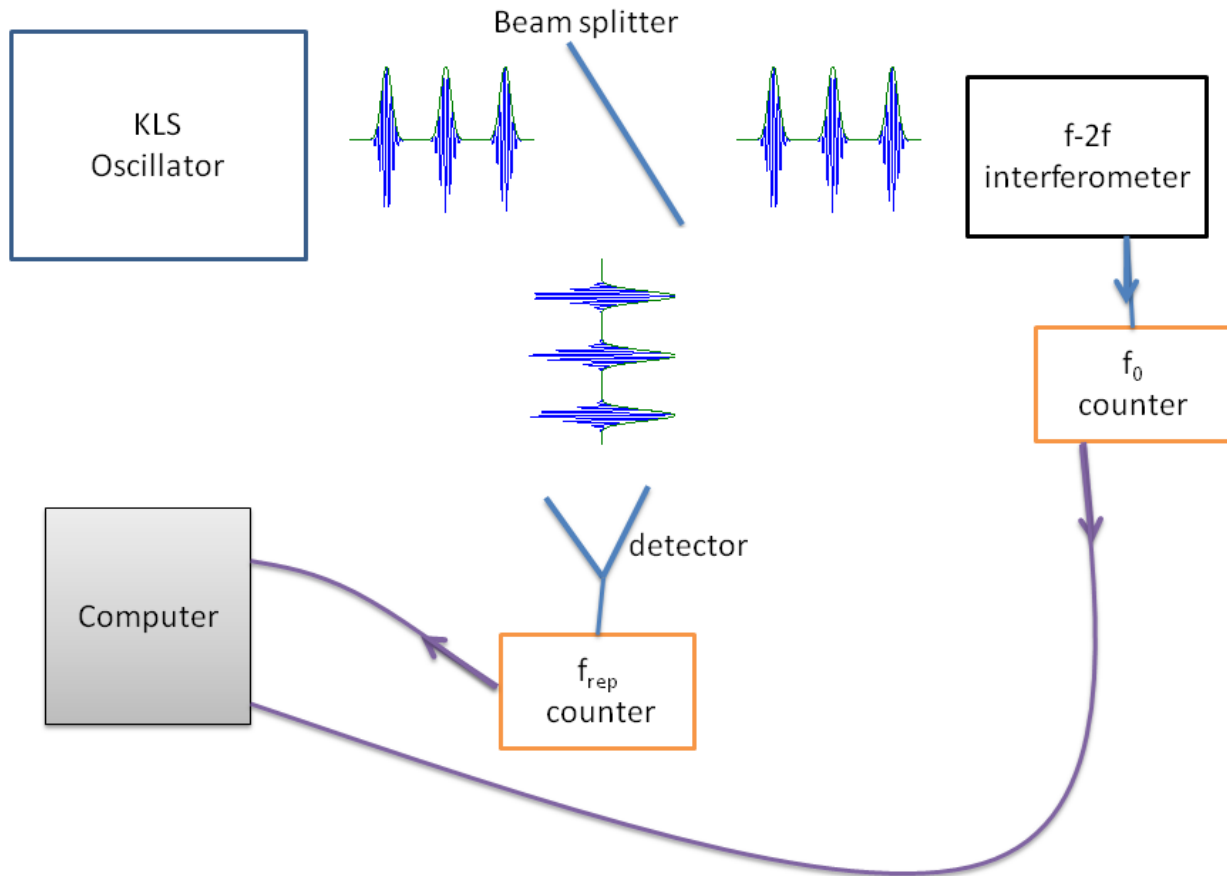
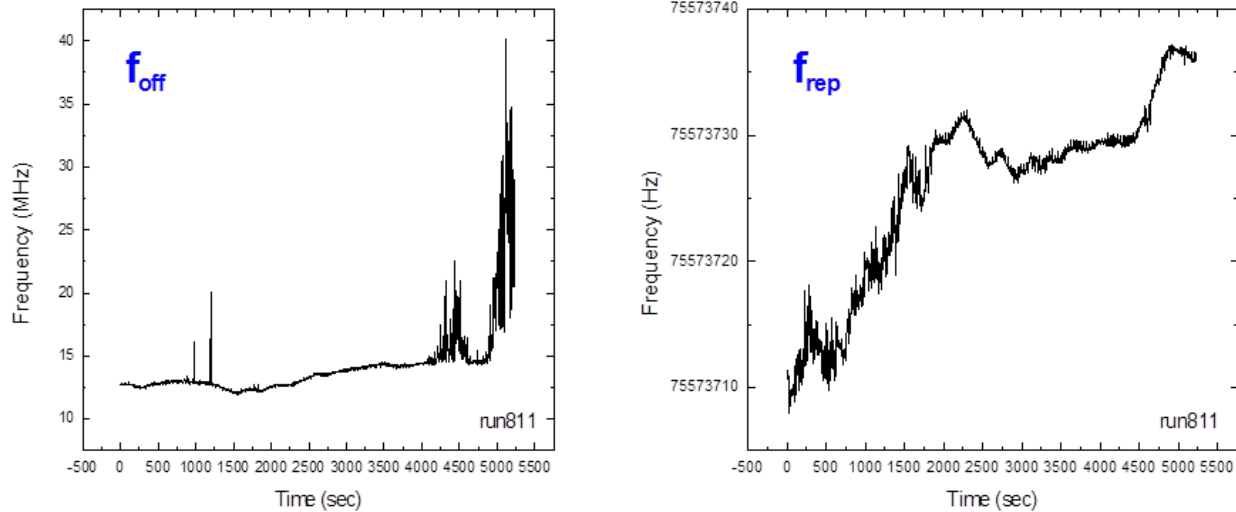


Figure 3.13: This is the same setup as Fig. 3.12, but with no ion detection. Pulses were split in half. 50% was sent to the $f-2f$ interferometer for the f_{off} measurement, and the rest was sent to a fast photo-detector for the f_{rep} measurement.

Fig. 3.14.

f_{rep} and f_{off} as a function of time



f_{off} scanning range is 2 MHz

f_{rep} scanning range is 30 Hz
 nf_{rep} scanning range is 110 MHz

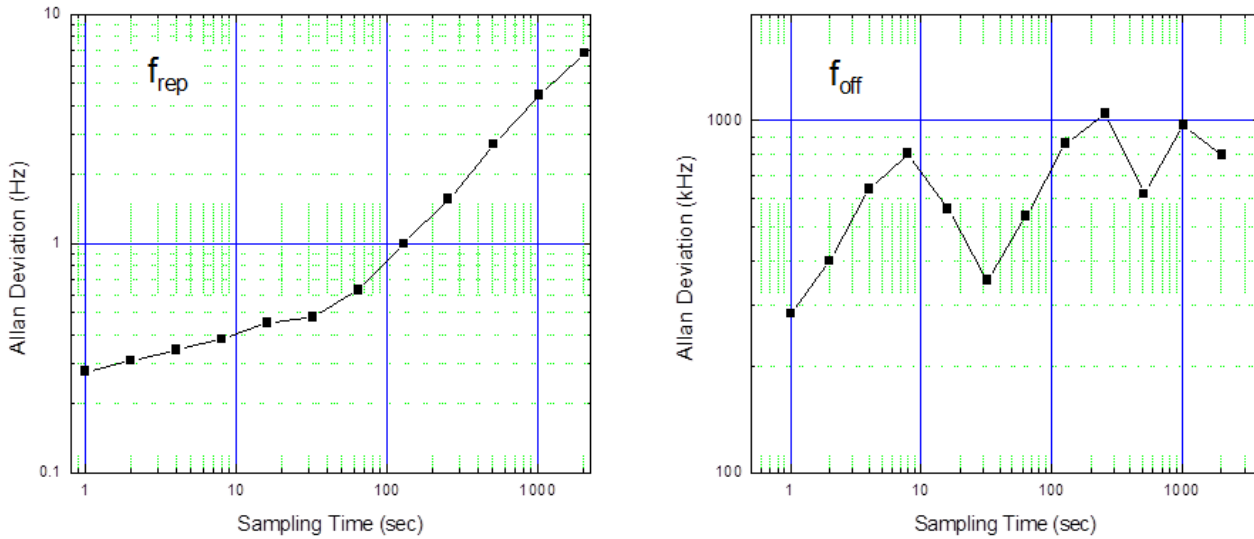
Figure 3.14: This is a plot to demonstrate how f_{off} and f_{rep} change in time. In this case only 2 hours of data are presented.

As we can see from these data, the scanning range for f_{rep} is 30 Hz and the scanning range for f_{off} is 2 MHz in about 2 hours. Since the frequency of a tooth equals $nf_{\text{rep}} - f_{\text{off}}$, where n is on the order of 10^6 , this gives us about 110 MHz scanning range for a tooth, which completely covers all the hyperfine transitions of the Rb atoms for the manifolds under study.

As for the second question, is the laser stable in this 100 ms interval? We took the above data and applied the Allan deviation formula,³⁵ which is a tool for estimating the stability

of data: $\sigma_f(\tau) = \sqrt{\frac{1}{2}\langle(f_{n+1} - \bar{f}_n)^2\rangle}$, where τ is the sampling time and \bar{f}_n is the n^{th} frequency averaged over this sampling time.

Stability of f_{rep} and f_{off}



$$f_n = n f_{\text{rep}} - f_{\text{off}}$$

$$n \sim 5.1 \cdot 10^6$$

$$\sigma_{f_n} = \sqrt{n^2 \sigma_{f_{\text{rep}}}^2 + \sigma_{f_{\text{off}}}^2}$$

$$\sigma_{f_n} \sim 1 \text{ MHz}$$

Figure 3.15: This is a plot to estimate how stable f_{off} and f_{rep} are in different sampling times. The calculation below the figure was done for a 1 second sampling time.

In Fig. 3.15 we plot the Allan deviations in f_{rep} and f_{off} as functions of the sampling time. We see that in a 1 second sampling time, the maximum deviation in f_{rep} was under 0.3 Hz and for f_{off} the deviation was under 300 kHz. This gives an uncertainty in comb tooth frequency of less than 1.7 MHz. Furthermore, if we extrapolate the Allan deviation in f_{rep} down to 100 msec, the shortest period over which our counters can sample with adequate precision, we would expect an Allan deviation of about 0.2 Hz, leading to a comb tooth

uncertainty of about 1 MHz. This is not much broader than the 0.7 MHz line width³⁶ of the states in the $5d$ manifold of Rb.

3.4 Data Acquisition

Our data acquisition system was very simple. As we described earlier we only needed to record three signals in a 100 ms window: A signal from the repetition frequency counter, a signal from the offset frequency counter, and the number of ions that were produced. For this purpose we wrote a simple LabView code that read these signals and wrote them into 3 dimensional arrays.

Repetition and offset frequencies were read with Agilent Universal Frequency Counters.³⁷ These counters have a GPIB output port and with GPIB -USB converters the frequencies were read by the LabView code, running on a computer running Windows.

As for the ion counts, the signal from the PSD was converted into a NIM logic pulse using a constant fraction discriminator (CFD). The NIM pulse was then converted into a TTL pulse using a NIM-to-TTL converter and sent to the computer using a National Instruments 12 bit DAQ box (NI USB-6008). A simple schematic for this data acquisition system is shown in Fig. 3.16. The LabView code is shown in the appendix B.

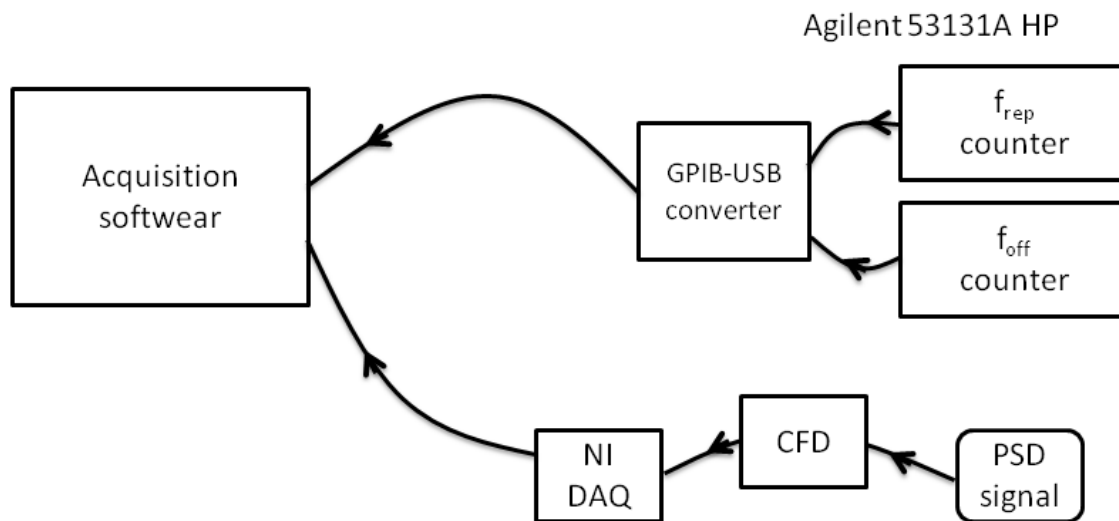


Figure 3.16: *Data acquisition scheme. Signals from f_{off} and f_{rep} counters were sent to the computer through a GPIB-USB converter. The ion signal from the PSD was read in through the CFD-NI DAQ.*

Chapter 4

Experimental Results

In this chapter we present the results of our experiments. As we mentioned in the introduction section our emphasis here was not to do an ultra high precision measurement but rather to see whether the ionization signal is significant when doing DFCS, and if it is, then see if one can learn the structure of the target system by looking at the ion signal as a function of f_{rep} and f_{off} . Therefore we didn't address issues that most of the high precision measurement groups do, such as turning off the MOT magnetic fields, that would allow us to ignore Zeeman broadening effects, or decreasing the intensity of the laser to reduce power broadening, or turning off the RIMS electric field to eliminate Stark splitting effects, or even turning off the trapping and repump lasers while the frequency comb is hitting the target to make sure that all the atoms are in the $5s_{1/2}, F = 2$ ground state.

This chapter we divided into two parts. In the first part we show our binned experimental data and explain how the binning process was carried out. In the second section we show the results from a different perspective where we take advantage of the repetition of the structure in f_{rep} and f_{off} and add the cycles. In the same section we compare our experimental results to those predicted by our theoretical code and we draw our conclusions.

4.1 Binned 2D Plot of Our Experimental Results

Figure 4.1 shows a typical experimental result. This represents 130 minutes of data collection with an average laser power of 25 mW, focused to a beam diameter of 5.7×10^{-4} m. (See

appendix A for more details). The laser pulse width was 50 fs. The density (color) in the figure gives the average ion count rate at each set of parameters f_{rep} and f_{off} . Since the laser was allowed to drift passively, f_{rep} and f_{off} do not necessarily fill out the full phase space represented in the plot, i.e. a zero count rate could mean that no ions were generated when the laser was in that range, or it could mean that the laser never drifted into the range represented. The data from the experiment are made up of a stream of three-value vectors, each accounting for 100 msec of elapsed time. The vectors are composed of an f_{rep} measurement, an f_{off} measurement, and the number of ion counts accumulated during the measurement period. The data are then run through a routine (appendix C) that divides the parameter space into bins of width 0.1 Hz in f_{rep} and 2 MHz in f_{off} and sums the ion counts into the appropriate bin as each datum is read. After binning, the ion count total in each bin is divided by the number of data points that were summed into that bin in order to get the ion production rate. These ion production rates are plotted in Fig. 4.1. This spectrum was extremely reproducible over many runs taken months apart.

Ionization in Fig. 4.1 appear as nearly vertical stripes. This is because of the relationship between f_{rep} and f_{off} expressed by Eq. 1.2. For a single-photon resonance at frequency f_t , all f_{rep} and f_{off} satisfying $nf_{\text{rep}} - f_{\text{off}} = f_t$ will produce enhanced ionization. Thus, resonances appear as lines with slope n in Fig. 4.1. For our laser, n is about 5.1×10^6 , so a change of 1 MHz in f_{off} would shift a resonance peak 0.2 Hz in f_{rep} . For two-photon resonances, the stripes will have slopes given by the average of the tooth orders for the two transition frequencies. In principle, we could determine n by fitting the two-dimensional data in Fig. 4.1. This would not yield very good precision in our case both because of our experimental resolution and because of the random nature of our parameter space coverage.

4.2 1D Plot in Comparison with Theory

We choose, for demonstration purposes, to condense the data to one dimension by projecting to the f_{rep} axis along diagonals of slope n . We further choose to project to the arbitrary

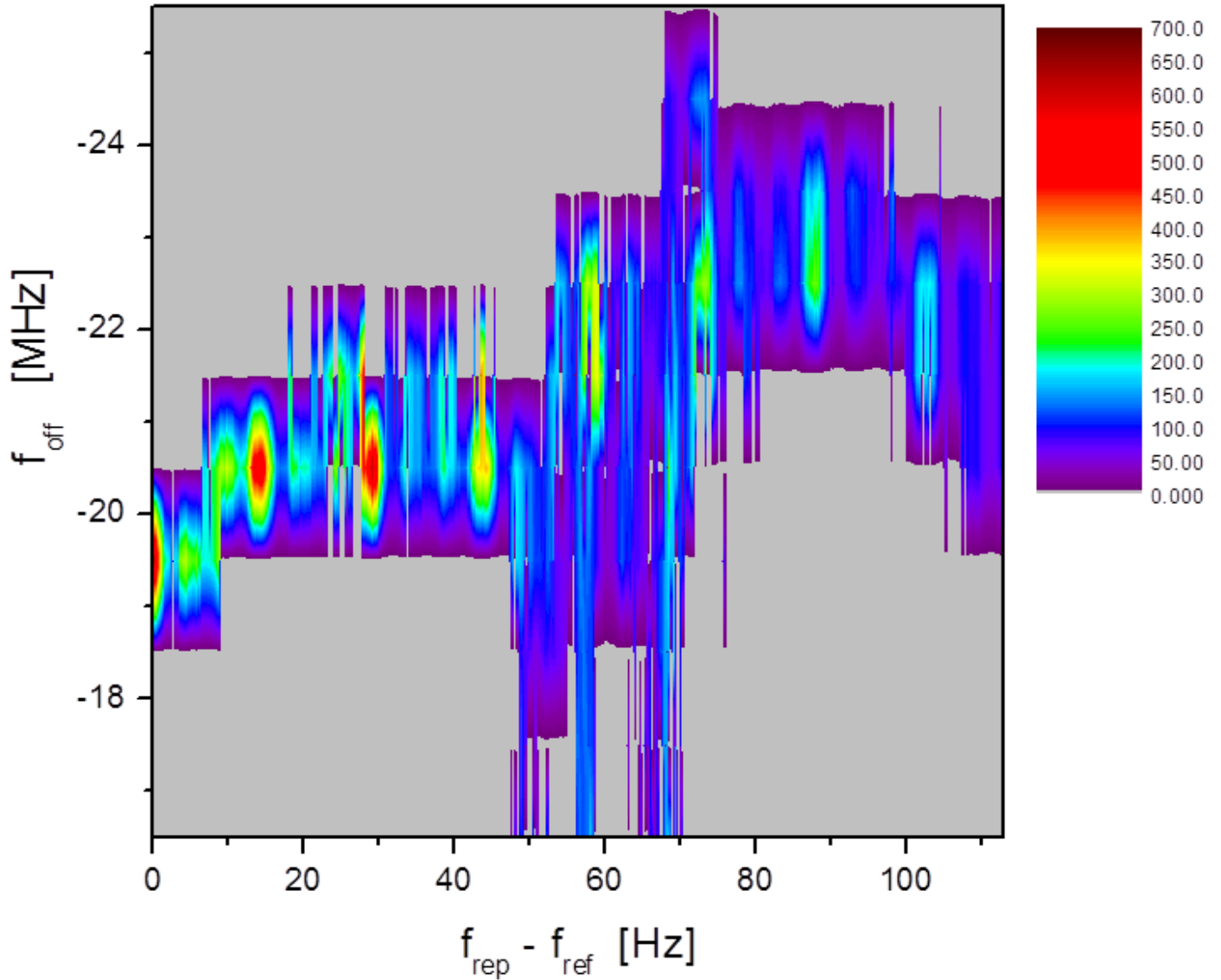


Figure 4.1: Plot of rubidium ion count rate, in ions per 100 ms, as a function of the freely varying parameters f_{rep} and f_{off} . $f_{\text{ref}} = 75616231$ Hz.

value of $f_{\text{off}} = -23.5$ MHz. A further compression of the data can be made by noticing that Eq. 1.2 is cyclic in the order n . Thus, if two repetition frequencies are related by $nf_1 = (n + 1)f_2$, both could excite the same atomic resonance, for constant f_{off} . For our laser a given one-photon transition should repeat at intervals of approximately 14.9 Hz in f_{rep} . We can, thus, combine repeated lines in our projected spectrum into a single range by cutting the f_{rep} axis at intervals of 14.9 Hz and shifting segments to the left by multiples of the cyclic interval (appendix C). Each ion rate is averaged over the number of segments combined this way. The projected data are shown in Fig. 4.2. The projection routine is not exact and contributes an additional width of approximately 0.1 Hz to the peaks in the DFCS scan, which is minor compared to the experimental resolution of 1 Hz. We note that this kind of analysis is not needed in active DFCS since there is no reason to simultaneously scan both f_{rep} and f_{off} ; nor is it necessary to scan f_{rep} over multiple orders.

The solid curve in Fig. 4.2 is from the measured ion rates, while the crosses are theoretical calculations, the latter plotted with an arbitrary vertical axis. The theory is the same as used for Fig. 2.2, but with the laser power set to the experimental value and f_{rep} and f_{off} also matched to the range of the measurements.

From Fig. 4.2 we can see that we obtain a large ionization rate, clearly adequate for spectroscopic measurements. There is also clear structure in the graph that is consistent with the calculated ionization spectrum. The differences between theory and experiment are due to the trapping laser being left on. For example, the apparent shift of some of the experimental peaks toward lower frequencies (near 2Hz) and higher frequencies (near 13 Hz) are actually due to enhanced excitation of the $5p_{3/2}, F = 3$, due to the trapping laser. In other words the peaks correspond to excitation with frequency teeth from $5p_{3/2}, F = 3$ to the allowed $5d$ hyperfine states, which are then ionized by any photon in the comb.

Considering all of these factors we can conclude that the theory and experiment agree very well.

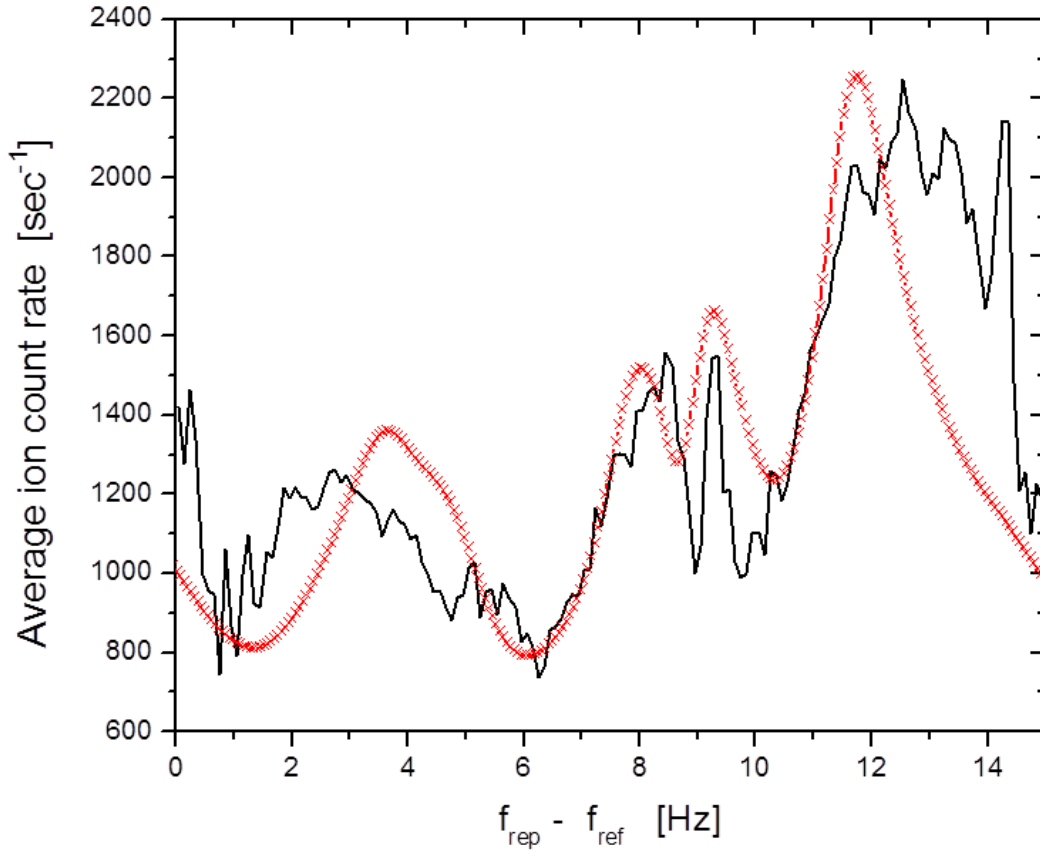


Figure 4.2: The data from Fig. 4.1 (solid black line). The ion count rates have been averaged over the cycles in f_{rep} and f_{off} and plotted versus $f_{\text{rep}} - f_{\text{ref}}$, where $f_{\text{ref}} = 75616232$ Hz. Also plotted is the calculated ion signal rate (crosses connected by a line). For both theory and experiment $f_{\text{off}} = -23.5$ MHz.

Chapter 5

Conclusion and Future Possibilities

In this chapter we give a brief summary of both theoretical and experimental results that were discussed in this dissertation. Then in the following section we point out some interesting ideas for future theoretical and experiential work.

5.1 Summary

As we pointed out earlier, this work mainly was motivated with two questions:

- First, we wanted to understand whether the ionization process was negligible compared excitation when doing DFCS.
- Second if the ionization signal was strong enough, we wanted to see if this signal could be used for studying the structure of the system of interest.

5.1.1 Theory

We adopted a theoretical model developed by Felinto that (in his case) was used to calculate the excited state populations of a target system while interacting with a frequency comb, as a function of the repetition frequency of a the comb. Since our goal was ionization we added continuum states to this model. We applied our code to ^{87}Rb atoms. The manifolds of interest were $5s$, $5p$, $5d$ and the continuum. Results of the calculations showed us that the ionization signal is actually greater than the $5d$ population. And at the same time it

showed us that everywhere we had a peak in the populations of the $5d$ states, we had the corresponding peak in the ionization signal, which answers the second question – at least theoretically.

We also showed that direct two photon ionization from the $5p$ states was negligible, which was the result of having a small population in the $5p$ excited states after interacting with the frequency comb. We tried to increase the population of the $5p$ states by increasing the intensity of the laser pulses, but it turned out that it actually had a negative effect, because of the process called optical pumping. The optical pumping is the effect of accumulating the populations in a so-called “dark” state, meaning none of the frequency comb teeth can resonantly excite a transition to any excited states from that state. At the same time we showed that with the same frequency comb one can undo the optical pumping, by choosing the appropriate repetition frequency and offset frequency. That basically means, while one tooth does optical pumping, another tooth re-pumps atoms from the dark state into the active ground state, much in the same way that our MOT repump works.

We also decided to see how the $5d$ excited state populations change as a function of chirp (both positive and negative). We considered two types of two photon transitions: One resonant with transition to the intermediate states (Type A) and a second not being resonant with transition to the intermediate states (Type B). The result showed us that in the case of type B transitions, the excitation was enhanced by a factor of 100 for both positive and negative chirp compared to the result with transform limited pulses. As for the Type A transitions, the negative chirp showed decreasing excitation amplitude whereas a positive chirp increased it. These results are in good agreement with 2nd order perturbation theory.

Last we looked at the effect of decreasing the number of pulses interacting with the system on the excited state populations. The idea was to decrease the number of pulses in the train without affecting the structure, so that computation could be done more readily. The results were satisfactory as we managed to obtain the same structure with a greatly

reduced number of pulses in a train. This means that future computations can be made much more efficiently in terms of computer time.

5.1.2 Experiment

Next we decided to address the two questions experimentally. We used a ^{87}Rb MOT as the target system in order to eliminate the Doppler broadening effect. This target was subjected to an “infinite” train of pulses. All the ions that were produced in the interaction region were collected with RIMS spectrometer and counted using an ion detector.

Since our oscillator didn’t have the repetition frequency and offset frequency locking capability (which is necessary for doing DFCS) we used a different approach. We counted the ions produced in 100 ms window while reading the repetition and offset frequencies of the pulses that caused the ionization. In other words we were doing DFCS only 100 ms at a time, but for good statistics our experiments ran for hours. It was estimated that within this 100 ms window the laser repetition and offset frequency were very stable. As the temperature was changing in the laser room so were the repetition and offset frequencies, which was equivalent to scanning them, although not uniformly in time. Then the ion counts were plotted as a function of repetition and offset frequency. After sophisticated analysis we showed that the ionization signal was significant and it showed the level structure of the Rb atoms.

Unfortunately the resolution in our spectra is not very good. Our goal was to demonstrate the strength of the ionization channel rather than the resolution for which frequency comb spectroscopy is already known. By following the standard procedure of taking a series of measurements with gradually lower comb laser power and then extrapolating those spectra to zero intensity we would eliminate power broadening effects. Furthermore, if high resolution were our goal, we could have taken the pains to chop the trap’s B-field gradient, thereby eliminating Zeeman broadening.

While our data were in satisfactory agreement with theory, there were some discrepancies.

These were caused by processes due to the trapping lasers, and were therefore irrelevant to the hypothesis we were testing. Just as in the case of the B-field gradient, the trapping laser could have been chopped to eliminate these effects, though the starting point in the comb laser excitation would still have been with optically pumped rubidium in the ground state. The loss in duty cycle would have simply given rise to reduced counting statistics.

Finally, we also demonstrated a novel implementation of DFCS in which f_{rep} and f_{off} were not controlled, but were varied through the natural interaction of the laser system and the changing ambient temperature. Our assessment of this passive comb is that, while workable, it has significant disadvantages over a conventional comb. The most serious of these is that one cannot simply dial in a tooth frequency of interest. Thus, we could not look for double resonances, in which one comb tooth was resonant with a transition between the $5s$ and $5p$ manifolds, while another tooth was resonant with a transition between the $5p$ and $5d$ manifolds. This makes it virtually impossible to use a passive comb to investigate, for example, optical pumping effects. Nevertheless, for laboratories that have an ultrafast oscillator but no true comb, impromptu passive comb experiments could still be done. We would like to emphasize here that the way we did our experiment doesn't have any advantage over DFCS experiment with a real comb, except that we showed that one need not have an actively stabilized comb laser to do DFCS.

5.2 Future Possibilities

Even though we did a lot of calculations and obtained lots of interesting results both theoretically and experimentally, there is still a lot to be done in this field.

First of all it would be very interesting to watch the population evolution on a time scale of ns, which is the time between two successive pulses in the train, basically to see how the population changes from pulses to pulse to pulse. We could do this theoretically since we already have a well developed code, and experimentally using our MOTRIMS apparatus.

Also the frequency range for a given frequency comb laser is limited; furthermore there

are some frequency regions where frequency combs do not exist at all. This clearly limits the atomic and molecular species that can be detected. In the future our group plans to increase the useful domain of comb frequencies by using two separate combs having very different frequency ranges. Combining the light from these two different color combs will open the door to a wide range of opportunities such as detecting trace amounts of particles of nearly any kind, studying very complex molecules such as DNA, controlling and predicting the results of chemical reactions, contributing toward the development of a quantum computer, and detecting the position and velocity of distant objects. Detecting trace amounts of materials is especially interesting in terms of its potential for commercialization: Two color comb techniques can be used for security purposes to detect potential explosive and bio-hazards and toxic gases, and to investigate contaminated areas. In the medical field, the technique can be used as a diagnostic for a broad range of pathogens through breath analysis.

Our group's initial object of study will be atomic rubidium. This is an ideal test system because the study of its structure requires use of two frequency combs having wavelengths centered at 780 and 1529 nm. Furthermore, we are already optically trapping and cooling rubidium atoms down to 150 microKelvin using a Magneto Optical Trap. This eliminates all Doppler broadening effects, which would introduce complications in the interpretation of the data. Finally, rubidium atomic lines have already been studied with high precision, providing a benchmark against which we can compare our results, thereby allowing us to determine how good our new technique is.

Bibliography

- [1] J. Ye, H. Schnatz, and L. W. Holberg, IEEE Journal of Selected Topics in Quantum Electronics **9** (2003).
- [2] T. R. Schibli et al., Opt. Exp. **14**, 5984 (2006).
- [3] I. Coddington, W. C. Swann, and N. R. Newbury, Phys. Rev. Lett. **100(1)**, 013902 (2008).
- [4] J. Mandon, G. Gulelachvili, and N. Picque, Nature Photon **3**, 99 (2009).
- [5] T. Steinmetz et al., Science. , 1335 (2008).
- [6] F. Adler, M. J. Thorpe, K. C. Cossel, and J. Ye, Annual Review of Analytical Chemistry , 175 (2010).
- [7] M. C. Stowe et al., Adv. At. Mol. Opt. Phys. **55**, 1 (2008).
- [8] A. Marian, M. C. Stowe, J. R. Lawall, D. Felinto, and J. Ye, Science. **306**, 2063 (2004).
- [9] A. Marian, M. C. Stowe, D. Felinto, and J. Ye, Phys. Rev. Lett. **95**, 023001 (2005).
- [10] G. N. Gibson, R. Klank, and F. Gibson, Opt. Lett. **21** (1996).
- [11] G. P. Barwood, P. Gill, and W. R. C. Rowley, Appl. Phys. B **53**, 142.
- [12] J. Ye and S. T. Cundiff, *Femtosecond Optical Frequency Comb: Principle, Operation, and Applications*, Springer, 2005.
- [13] H. U. Jang et al., Phys. Rev. A **82**, 043424 (2010).
- [14] D. Felinto, L. H. Acioli, and S. S. Vianna, Phys. Rev. A **70**, 043403 (2004).

- [15] D. Felinto and C. E. E. López, Phys. Rev. A **80**, 013419 (2009).
- [16] This limitation can be somewhat relaxed through a different choice of format (binary rather than ASCII) in the numbers stored to disk between separate parts of the computation.
- [17] B. C. Duncan, V. Sanchez-Villicana, P. L. Gould, and H. R. Sadeghpour, Phys. Rev. A **63**, 043411 (2001).
- [18] We do not consider optical pumping between m_F states, for which polarization control is also needed.
- [19] N. Dudovich, B. Dayan, S. M. G. Faedar, and Y. Silberger, Phys. Rev. Lett. **86**, 47 (2001).
- [20] H. J. Metcalf and P. V. D. Straten, *Laser cooling and trapping*, Springer, 2001.
- [21] E. L. Raab, M. Prentiss, A. Cable, S. Chu, and D. E. Pritchard, Phys. Rev. Lett. **59**, 2631 (1987).
- [22] S. Chu and C. Wieman, J. Opt. Soc. Am. B **6**, 2020 (1989).
- [23] C. Wieman, G. Flowers, and S. Gilbert, Am. J. Phys. **63**, 317 (1995).
- [24] H. Jang, *Thesis Title*, PhD thesis, Kansas State University, Manhattan, KS, 2000, “<http://jrm.phys.ksu.edu/>”.
- [25] W. Demtröder, *Laser Spectroscopy: Basic Concepts and Instrumentation*, volume 2nd Ed., Springer, 1996.
- [26] K. B. MacAdam, A. Steinbach, and C. Wieman, Am. J. Phys. **60**, 1098 (1992).
- [27] W. Lu et al., Rev. Sci. Instrum. **67**, 3003 (1996).

- [28] Cross-over peaks appear halfway between two states that can be excited from the same lower state. In the 1-2 cross-over case, the lower state is $5s_{1/2}, F = 1$ and the two excited states are $5p_{3/2}, F = 1$ and $5p_{3/2}, F = 2$. Cross-overs appear because when the laser is tuned exactly halfway between two excited states there is precisely one non-zero velocity of the atoms for which the pump laser is resonant with one of the upper states while simultaneously the oppositely propagating probe laser is resonant with the second state. Because the pump laser is resonant, the lower level is partially depleted. Therefore, *for that same narrow velocity group only*, the probe beam is absorbed less and yields a Doppler-free signal.
- [29] X. Fléchar, H. Nguyen, E. Wells, I. Ben-Itzhak, and B. D. DePaola, Phys. Rev. Lett. **87**, 123203 (2001).
- [30] H. Nguyen, X. Fléchar, R. Brédy, H. A. Camp, and B. D. DePaola, Rev. Sci. Instrum. **75**, 2638 (2004).
- [31] D. J. Jones et al., Science. (2000).
- [32] R. Holzwarth, T. Udem, and T. W. Hansch, Phys. Rev. Lett. **85**, 2264 (2008).
- [33] Photonic Crystal Fiber. “http://en.wikipedia.org/wiki/Photonic-crystal_fiber”.
- [34] Kerr effect, self phase modulation. “http://en.wikipedia.org/wiki/Self-phase_modulation”.
- [35] Allan variance. “http://en.wikipedia.org/wiki/Allan_variance”.
- [36] O. S. Heavens, J. Opt. Soc. Am. **51**, 1058 (1961).
- [37] Hewlett Packard Model 53131A Counter.
- [38] G. Veshapidze, M. L. Trachy, M. H. Shah, and B. D. DePaola, Appl. Opt. **45**, 8197 (2006).

[39] C. J. Hawthorn, K. P. Weber, and R. E. Scholten, *Rev. Sci. Instrum.* **72** (2001).

Appendix A

Estimating the Laser Beam Size

The spot size of the laser beam was estimated with an edge-scanning method.³⁸ This process was done in free space at the focus of the identical lens that was used to focus the laser beam inside the MOT chamber. The results of this measurement are shown in Fig. A.1. The black line represents the derivative of the data and the red line is a fitted Gaussian. From the fit we see that the FWHM of the beam is about 5.7×10^{-4} m.

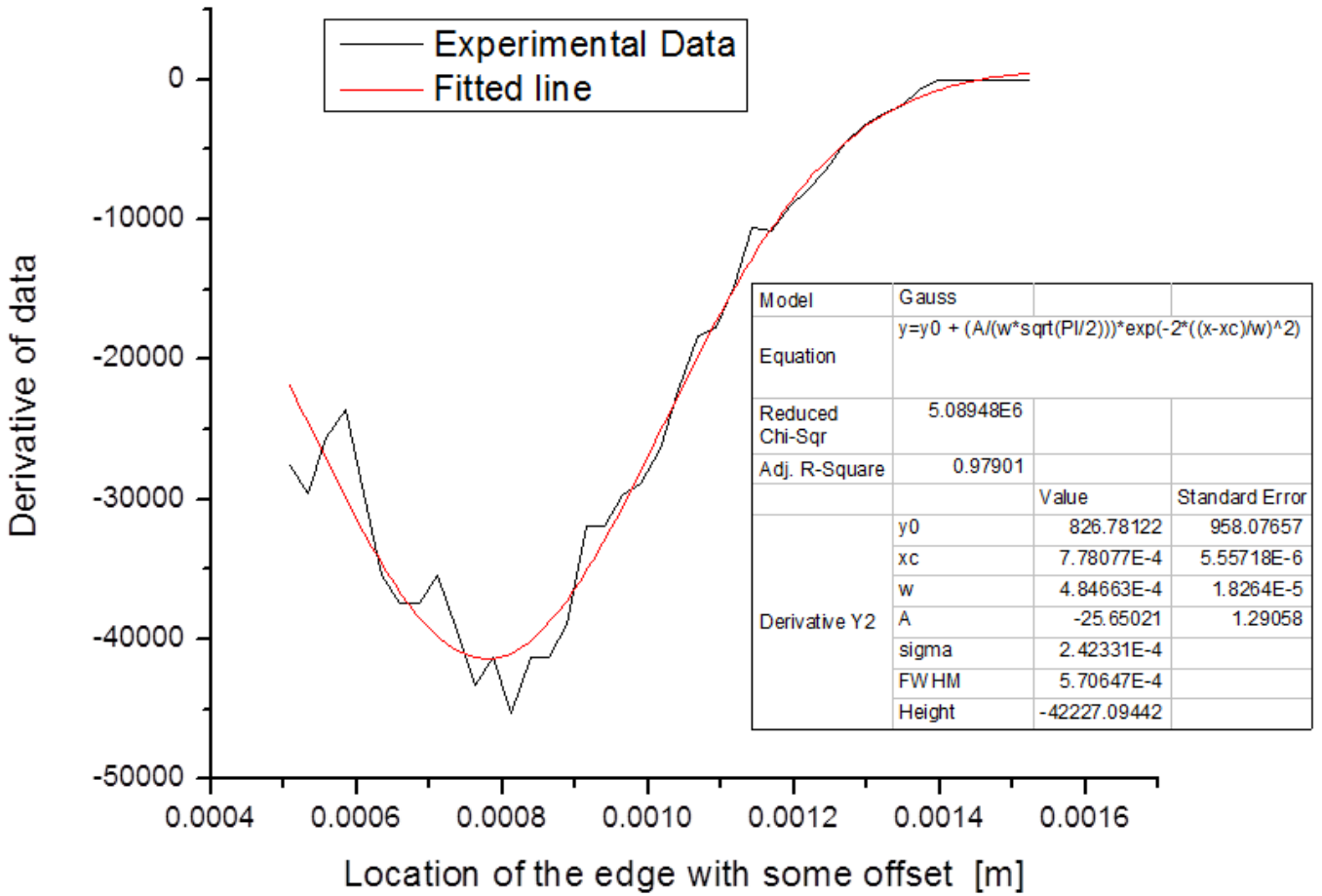


Figure A.1: Here we estimate size of the beam using the so-called knife-edge method. The black line is data, and the red line is a fitted Gaussian.

Appendix B

Labview Program for Data Acquisition

Below is the labview code that was used for data acquisition. The code (main structure) was written by Vince Needham and later was modified by me. This code reads in three signals, two from the frequency counters and the third from the PSD, and it stores them in three columns.

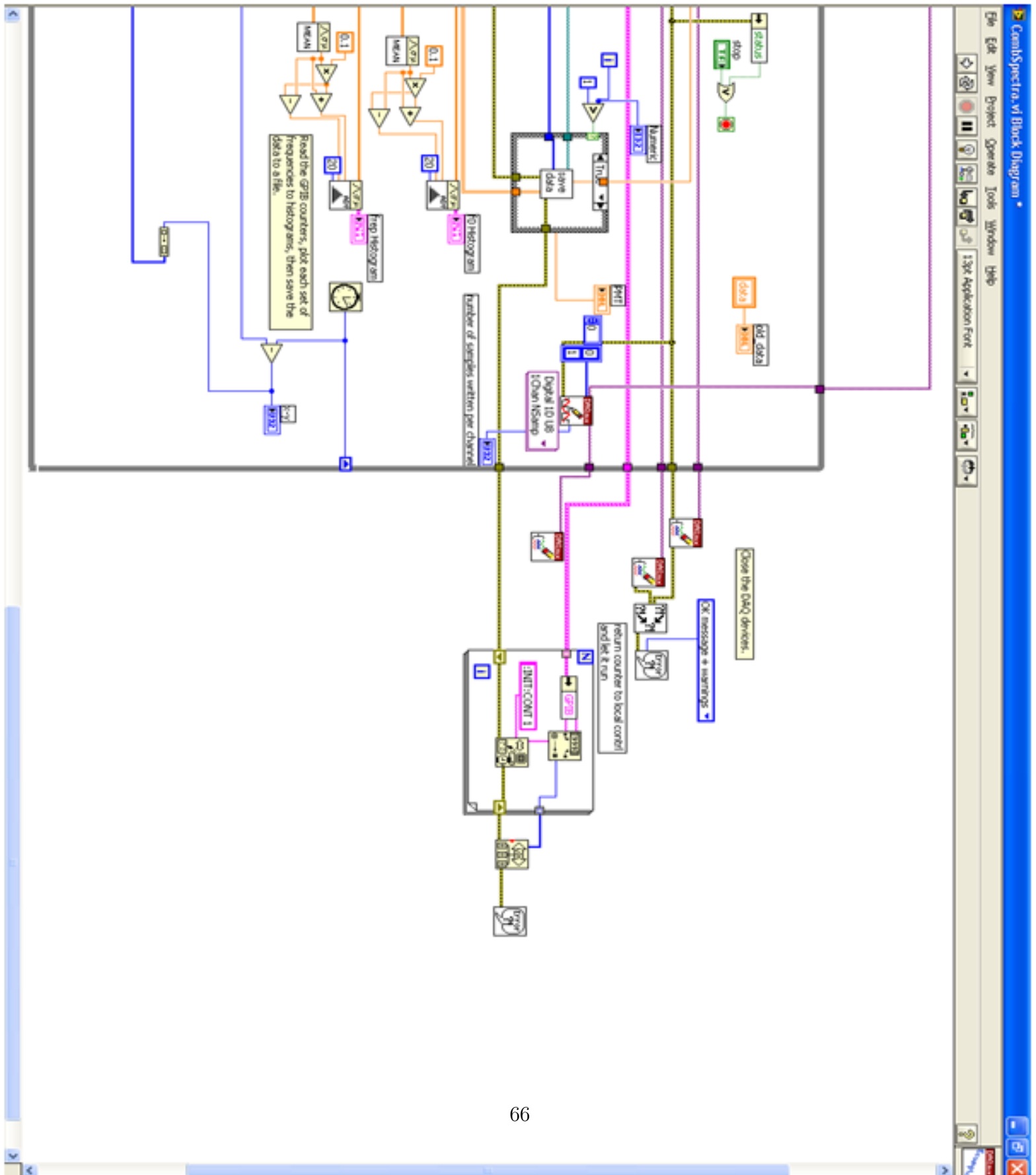


Figure B.2: LabView code2.

Appendix C

Binning-Program

Here we show the programs used to add cycles in f_{rep} and f_{off} and then bin the results.

```
// Global Stuff:

// Libraries:
#include <iostream> #include <fstream> #include <string> #include
<cstring> #include <cstdlib> #include <vector>

using namespace std;

// Global Constants & Variables:

ifstream in_stream;
ofstream out_stream;

int main() {
    vector<double> cntin;
```

```

vector<double> f0in;
vector<double> fRin;
vector<double> f0_out;
vector<double> fR_out;
vector<double> cnts_out;
vector<double> norm_out;
vector <double> fin_norm;
vector <double> bin_norm;
vector<double> average;
vector<int> mod;

double cnts,f0,fR,pmt,fRmin,fRmax,f0min,f0max,dfR,df0, fofflow, foffhigh;
double fmintmp,fmaxtmp;
int numf0,numfR;
int Nraw=0,fint,lenout,Nout=0;
int r,r1,r2, r3,r4,m,l;
char infilenam[30],outfilenam[30], binned;
char dummy; // use this for debugging

// set the precisions for output to the screen:
cout.setf(ios::fixed);
cout.setf(ios::showpoint);
cout.precision(5);

// input the raw data; find mins, maxs and numlines of data:

```

```

//cout<<"\n What is the name of the output file (with an extension)?\n";
// cin>>outfilenam;
in_stream.open("comb052711D.dat"); // open the raw data file
// in_stream.open(infilenam); // open the raw data file
if((in_stream.fail())) // make sure file can be found
{
    cout<<"Input file opening failed.\n";
    exit(1);
}
in_stream>>cnts>>f0>>fR>>pmt; //read in first line of file

//find min and max
fRmin=fR;
fRmax=fR;
f0min=f0;
f0max=f0;
cntin.push_back(cnts);
f0in.push_back(f0);
fRin.push_back(fR);

while (!in_stream.eof())
{
    in_stream>>cnts>>f0>>fR >>pmt;
    if(fR>fRmax){fRmax=fR;}
    if(fR<fRmin){fRmin=fR;}
    if(f0>f0max){f0max=f0;}
    if(f0<f0min){f0min=f0;}
}

```

```

        Nraw++;
        cntin.push_back(cnts);
        f0in.push_back(f0);
        fRin.push_back(fR);

    }

    in_stream.close(); // close raw data file

//output mins and maxes:
    cout << endl;
    cout << "min and max of fR: " << fRmin << " " << fRmax << endl;
    cout << "min and max of f0:  " << f0min << " " << f0max << endl;
    cout << "number of lines of data: " << Nraw << endl;

// these are default values:
    // fRmin=75557551;
    // fRmax=75557616;
    // f0min=5000000;
    // f0max=15000000;

//fn=nfrep-f0; fix one f0 and shift all other f0 respect to it,
//shiftnng means changing frep.

//
    for (int i=0; i<= Nraw; i++)
    {
        fRin[i]=(fRin[i]+(23500000-f0in[i]))/(5.1e6);
    }

```

```

        f0in[i]=f0in[i];
    }

//after shifting find min value of frep and subtract it from all the
//frep

double min=fRmax;
for (int i=0; i<=Nraw; i++)
{

if (min > fRin[i]) { min =fRin[i];}

}

cout<<min;

for (int i=0; i<= Nraw; i++)
    {
        fRin[i]=fRin[i]-min;
    }

for (int i=0; i<= Nraw; i++)
    {

mod.push_back(0);
f0_out.push_back(0.0);
fR_out.push_back(0.0);

```

```

}
//adding cycles in frep
for (int i=0; i<= Nraw; i++)
    {
mod[i]=fRin[i]/14.91; fR_out[i]=fRin[i]-mod[i]*14.91;
f0_out[i]=23500000;
//cout<< fR_out[i]<<endl;
}

//output of the program
out_stream.open("comb_shifted.dat");
// out_stream.open(outfilenam);

// set the precisions for output to a file:
out_stream.setf(ios::fixed);
out_stream.setf(ios::showpoint);
out_stream.precision(6);

for (int i=0; i<Nraw; i++)
out_stream<<cntin[i]<< " " << f0_out[i]<< " " << fR_out[i]<<" "<<cntin[i]<< endl;
out_stream.close();
}

```

The next program uses the output of the previous code and bins it.

```

// Global Stuff:

// Libraries:
#include <iostream> #include <fstream> #include <string> #include
<cstring> #include <cstdlib> #include <vector>

using namespace std;

// Global Constants & Variables:

ifstream in_stream;
ofstream out_stream;

int main() {
    vector<double> cntin;
    vector<double> f0in;
    vector<double> fRin;
    vector<double> f0_out;
    vector<double> fR_out;
    vector<double> cnts_out;
    vector<double> norm_out;
vector <double> fin_norm; vector <double> bin_norm;
    vector<double> average;
    double cnts,f0,fR,pmt,fRmin,fRmax,f0min,f0max,dfR,df0, fofflow, foffhigh;
    double fmintmp,fmaxtmp;

```

```

int numf0,numfR;
int Nraw=0,fint,lenout,Nout=0;
int r,r1,r2, r3,r4,m,l;
char infilenam[30],outfilenam[30], binned;
char dummy; // use this for debugging

// set the precisions for output to the screen:
cout.setf(ios::fixed);
cout.setf(ios::showpoint);
cout.precision(2);

// input the raw data; find mins, maxs and numlines of data:

    cout<<"What is the name of the file to bin (with an extension)?\n";
    cin>>infilenam;
    cout<<"\n What is the name of the output file (with an extension)?\n";
    cin>>outfilenam;
// in_stream.open("comb052811A.dat"); // open the raw data file
    in_stream.open(infilenam); // open the raw data file
if((in_stream.fail())) // make sure file can be found
    {
        cout<<"Input file opening failed.\n";
        exit(1);
    }

in_stream>>cnts>>f0>>fR>>pmt; //read in first line of file
fRmin=fR;
fRmax=fR;

```

```

f0min=f0;
f0max=f0;
cntin.push_back(cnts);
f0in.push_back(f0);
fRin.push_back(fR);

while (!in_stream.eof())
{
    in_stream>>cnts>>f0>>fR >>pmt;
    if(fR>fRmax){fRmax=fR;}
    if(fR<fRmin){fRmin=fR;}
    if(f0>f0max){f0max=f0;}
    if(f0<f0min){f0min=f0;}
    Nraw++;
    cntin.push_back(cnts);
    f0in.push_back(f0);
    fRin.push_back(fR);
}
in_stream.close(); // close raw data file

//output mins and maxes:
cout << endl;
cout << "min and max of fR: " << fRmin << " " << fRmax << endl;
cout << "min and max of f0:  " << f0min << "  " << f0max << endl;
cout << "number of lines of data: " << Nraw << endl;

// these are default values:

```

```

// fRmin=75557551;
// fRmax=75557616;
// f0min=5000000;
// f0max=15000000;

// input ranges and bin sizes:
cout << endl;
    cout << "Input minimum and maximum values of fR you are interested in.\n";
    cout << "The default values are "<<fRmin<< " " <<fRmax<<endl;
    cout <<"(To use a default values, enter 0 for each that value)\n";
cin >> fmintmp >> fmaxtmp;
    if (fmintmp>0.0001) fRmin=fmintmp;
    if (fmaxtmp>0.0001) fRmax=fmaxtmp;

cout << endl;
cout << "Input minimum and maximum values of f0 you are interested in.\n";
    cout << "The default values are "<<f0min<< " " <<f0max<<endl;
    cout << "(To use a default values, enter 0 for that value)\n";
cin >> fmintmp >> fmaxtmp;
    if (fmintmp>0.0001) f0min=fmintmp;
    if (fmaxtmp>0.0001) f0max=fmaxtmp;

// cout << "input the size of your frep (in Hz) and f0 (in Hz) bins.\n";
//cin >> dfR >> df0;
// cout <<endl;
// df0=df0 *1.0e6;
dfR=0.1;

```

```

df0=1000000;
// bin the data:
    for (int i=0; i<= Nraw; i++)
        {
            fint=fRin[i]/dfR;
            fRin[i]=(fint+0.5)*dfR;
            fint=f0in[i]/df0;
            f0in[i]=(fint+0.5)*df0;
            //    cout <<f0in[i] << ' ' << fRin[i]<< endl;
        }

// create output data:
    numf0=(f0max-f0min)/df0;
    numfR=(fRmax-fRmin)/dfR;
    lenout=(numf0+1)*(numfR+1);
    cout<< "lenout, numf0, numfR= "<<lenout << " " <<numf0<<" " <<numfR<<endl;

// first initialize:
    for (int i=0; i<=lenout; i++)
        {
            f0_out.push_back(0.0);
            fR_out.push_back(0.0);
            cnts_out.push_back(0.0);
            norm_out.push_back(0.001);
        }

// now fill in the frequencies:
    for (int if0=0; if0<=numf0; if0++)

```

```

for (int ifR=0; ifR<=numfR; ifR++)
{
    f0_out[if0*(numfR+1)+ifR]=f0min+(if0+0.5)*df0;
    fR_out[if0*(numfR+1)+ifR]=(ifR+0.5)*dfR;
    Nout++;
}

cout<<"Nout= "<<Nout<<" lenout= "<<lenout<<endl;
// collapse the raw data into the new vectors:
for (int i=0; i<=Nraw; i++)
{
    if (( f0in[i]>=f0min)&(f0in[i]<=f0max)&(fRin[i]>=fRmin)&(fRin[i]<fRmax))
    {
        r1=(f0in[i]-f0min)/df0;
        r2=(fRin[i]-fRmin)/dfR;
        r=(numfR+1)*r1+r2;
        if((r<=Nout) & (r>=0))
        {
            cnts_out[r]=cnts_out[r]+cntin[i];
            norm_out[r]=norm_out[r]+1.0;
        }
    }
}

out_stream.open("comb2d.dat");
// out_stream.open(outfilenam);

// set the precisions for output to a file:

```

```
out_stream.setf(ios::fixed);
out_stream.setf(ios::showpoint);
out_stream.precision(6);

for (int i=0; i<Nout; i++)
    out_stream<<f0_out[i]<<" "<<fR_out[i]<<" "
        <<cnts_out[i]/norm_out[i]<<endl;
out_stream.close();
}
```

Appendix D

Identifying Structure Lines

Here we show the Matlab code that was used to identify $5d$ and $5p$ hyperfine energy lines in our theoretical and experimental data. In this code we specify what the offset frequency was for the laser and the range we scanned our laser repetition frequency and it calculates the position (in f_{rep}) for the teeth that cause 1 photon or two photon excitation to the $5p$ and $5d$ states correspondingly followed by ionization.

D.1 Two Photon Transition

Below is the code for the $5s$ to $5d$ transitions.

```
close all
clear all
clc
format long
foff=-23500000;
frepmin=75616304.25;
frepmax=frepmin+20;
```

```

load rho.dat %read in raw data

mat1=rho;

shift=6834682600;

% input all the transition frequencies from
% the 5s F=2 to the 5d hyperfine states.
D32F0=770487024638000-shift;
D32F1=770487038137000-shift;
D32F2=770487066067800-shift;
D32F3=770487110290200-shift;
D52F4=770569132732600;
D52F3=770575996238200-shift;
D52F2=770576019193000-shift;
D52F1=770576035133000-shift;

tran2=[D32F0 D32F1 D32F2 D32F3 D52F4 D52F3 D52F2 D52F1];
format long
for k=1:1:length(tran2)
% finding minimum and maximum teeth number for each transition.
topn(k)=floor((tran2(k)-2*foff)/frepmin);
to(k)=((tran2(k)-2*foff)/frepmin);
bottomn(k)=floor((tran2(k)-2*foff)/frepmax);
bot(k)=((tran2(k)-2*foff)/frepmax);

l=0;

```

```

% use the teeth numbers, increment it by one and find,
%where the repetition frequencies
%need to be to get an excitation with the teeth.
    for m=bottomn(k):1:topn(k)
        s=bot(k):1:to(k);
        l=1+1;
        frep(l,k)=(tran2(k)-2*foff)/m;
    end
end

yaxis=(1:topn(1)-bottomn(1)+1)*0+140;

D32F0=[(frep(:,1))-frepmin,yaxis'];
D32F1=[frep(:,2)-frepmin,yaxis'];
D32F2=[frep(:,3)-frepmin,yaxis'];
D32F3=[frep(:,4)-frepmin,yaxis'];
D52F4=[frep(:,5)-frepmin,yaxis'];
D52F3=[frep(:,6)-frepmin,yaxis'];
D52F2=[frep(:,7)-frepmin,yaxis'];
D52F1=[frep(:,8)-frepmin, yaxis']

%plot the input data and the lines describing which
% peak corresponds to which transition
subplot(2,1,1)

semilogy(mat1(:,1),mat1(:,6))%,mat(:,1),mat(:,5))
factor=10000000000000000000;

```

```

axis([0 20 min(mat1(:,6)) max(mat1(:,6))])

hold on
bar(D32F0(:,1),D32F0(:,2)./factor,0.00001,'g','edgecolor','g')
%if 0
bar(D32F1(:,1),D32F1(:,2)./factor,0.0001,'r','edgecolor','r')

bar(D32F2(:,1),D32F2(:,2)./factor,0.0001,'b','edgecolor','b')
bar(D32F3(:,1),D32F3(:,2)./factor,0.00001,'y','edgecolor','y')
bar(D52F1(:,1),D52F1(:,2)./factor,0.00001,'m','edgecolor','m')

bar(D52F2(:,1),D52F2(:,2)./factor,0.00001,'c','edgecolor','c')
bar(D52F3(:,1),D52F3(:,2)./factor,0.00001,'k','edgecolor','k')
bar(D52F4(:,1),D52F4(:,2)./factor,0.00001,'w','edgecolor',orange)
legend('data','D32F0','D32F1','D32F2','D32F3','D52F1','D52F2','D52F3','D52F4')

title('F=2')

% the same procedure but from 5s F=1 state to all the 5d hyperfine states.

clear all
clc
format long

foff=-23500000;

```

```
frepmin=75616304.25;
```

```
frepmax=frepmin+20;
```

```
shift=6834600000;
```

```
load rho.dat
```

```
mat1=rho;
```

```
shift=6834682600;
```

```
D32F0=770487024638000;
```

```
D32F1=770487038137000;
```

```
D32F2=770487066067800;
```

```
D32F3=770487110290200;
```

```
D52F4=770569132732600+shift;
```

```
D52F3=770575996238200;
```

```
D52F2=770576019193000;
```

```
D52F1=770576035133000;
```

```
tran2=[D32F0 D32F1 D32F2 D32F3 D52F4 D52F3 D52F2 D52F1]; format long
```

```
for k=1:1:length(tran2)
```

```
    topn(k)=floor((tran2(k)-2*foff)/frepmin);
```

```
    to(k)=((tran2(k)-2*foff)/frepmin);
```

```

    bottomn(k)=floor((tran2(k)-2*foff)/frepmax);
    bot(k)=((tran2(k)-2*foff)/frepmax);

l=0;

    for m=bottomn(k):1:topn(k)
        s=bot(k):1:to(k);
        l=l+1;

        frep(l,k)=(tran2(k)-2*foff)/m;

    end

end

%topn-bottomn
yaxis=(1:topn(1)-bottomn(1)+1)*0+140;
%yaxiss=(1:to(1)-bot(1)+0)*0+45;

D32F0=[(frep(:,1))-frepmin,yaxis'];
D32F1=[frep(:,2)-frepmin,yaxis'];
D32F2=[frep(:,3)-frepmin,yaxis'];
D32F3=[frep(:,4)-frepmin,yaxis'];
D52F4=[frep(:,5)-frepmin,yaxis'];
D52F3=[frep(:,6)-frepmin,yaxis'];
D52F2=[frep(:,7)-frepmin,yaxis'];
D52F1=[frep(:,8)-frepmin, yaxis']

```

```

subplot(2,1,2)

semilogy(mat1(:,1),mat1(:,6))%,mat(:,1),mat(:,5))
%factor=1000;

factor=1000000000000000000;

axis([0 20 min(mat1(:,6)) max(mat1(:,6))])

hold on
bar(D32F0(:,1),D32F0(:,2)./factor,0.00001,'g','edgecolor','g')
%if 0
bar(D32F1(:,1),D32F1(:,2)./factor,0.0001,'r','edgecolor','r')

bar(D32F2(:,1),D32F2(:,2)./factor,0.00001,'b','edgecolor','b')
bar(D32F3(:,1),D32F3(:,2)./factor,0.00001,'y','edgecolor','y')
bar(D52F1(:,1),D52F1(:,2)./factor,0.00001,'m','edgecolor','m')

bar(D52F2(:,1),D52F2(:,2)./factor,0.00001,'c','edgecolor','c')
bar(D52F3(:,1),D52F3(:,2)./factor,0.00001,'k','edgecolor','k')
bar(D52F4(:,1),D52F4(:,2)./factor,0.00001,'w','edgecolor',orange)
%legend('data','D32F0','D32F1','D32F2','D32F3','D52F1','D52F2','D52F3','D52F4')
%end

title('F=1')

```

D.2 One Photon Transition

And here we show the code for the 5s to 5p transitions

```
close all
clear all
clc

% this program is similar to the program above.
% It is written to identify all the peaks from the 5s to 5p states.
%
%s=0;
format long Eng
    foff=-23500000;
%s=s+1;
frepmin=75616304.25;

frepmax=frepmin+20;
%load comb053011Afull.dat
load rho.dat

%mat=comb053011Afull;
```

```

mat1=rho;
shift=6834682600;

P12F1=377111224728600-shift;
P12F2=377112041387600-shift;
P32F0=384234454070900-shift;
P32F1=384234526288900-shift;
P32F2=384234683235900-shift;
P32F3=384228115203300;

tran1=[P12F1 P12F2 P32F0 P32F1 P32F2 P32F3];

for k=1:1:length(tran1)

    topn(k)=floor((tran1(k)-foff)/frepmin);

    bottomn(k)=floor((tran1(k)-foff)/frepmax);

l=0;
    for m=bottomn(k):1:topn(k);
        l=l+1;
        frep(l,k)=(tran1(k)-foff)/m;

    end
end

topn-bottomn; yaxis=(1:(topn(1)-bottomn(1)+1))*0+140;

```

```

P12F1=[(frep(:,1))-frepmin,yaxis'];
P12F2=[frep(:,2)-frepmin,yaxis'];
P32F0=[frep(:,3)-frepmin,yaxis'];
P32F1=[frep(:,4)-frepmin,yaxis'];
P32F2=[frep(:,5)-frepmin,yaxis'];

P32F3=[frep(:,6)-frepmin,yaxis'];

subplot(2,1,1)

%plot(mat(:,2),mat(:,3),mat1(:,1),mat1(:,2)*15*10^3 )

%,mat(:,1),mat(:,5))
factor=1000000000000;

semilogy(mat1(:,1),mat1(:,6)) axis([0 20 min(mat1(:,6))
max(mat1(:,6))])

hold on
bar(P12F1(:,1),P12F1(:,2)./factor,0.000001,'g','edgecolor','g')

bar(P12F2(:,1),P12F2(:,2)./factor,0.000001,'r','edgecolor','r')

bar(P32F0(:,1),P32F0(:,2)./factor,0.000001,'b','edgecolor','b')
bar(P32F1(:,1),P32F1(:,2)./factor,0.000001,'y','edgecolor','y')
bar(P32F2(:,1),P32F2(:,2)./factor,0.000001,'m','edgecolor','m')

```

```

bar(P32F3(:,1),P32F3(:,2)./factor,0.00001,'c','edgecolor','c')
%bar(D52F3(:,1),D52F3(:,2)./factor,0.00001,'k','edgecolor','k')
%bar(D52F4(:,1),D52F4(:,2)./factor,0.00001,'w','edgecolor',orange)
legend('data1','P12F1','P12F2','P32F0','P32F1','P32F2','P32F3')

title('F=2')

%legend('5p','5d','cont')

clear all clc

format long Eng
    foff=-23500000;
%s=s+1;
frepmin=75616304.25;

frepmax=frepmin+20;
%load comb053011Afull.dat
load rho.dat

%mat=comb053011Afull;

mat1=rho;
shift=6834682600;
P12F1=377111224728600;

```

```

P12F2=377112041387600;
P32F0=384234454070900;
P32F1=384234526288900;
P32F2=384234683235900;
P32F3=384228115203300+shift;

tran1=[P12F1 P12F2 P32F0 P32F1 P32F2 P32F3];

for k=1:1:length(tran1)
    topn(k)=floor((tran1(k)-foff)/frepmin);
    bottomn(k)=floor((tran1(k)-foff)/frepmax);

l=0;
    for m=bottomn(k):1:topn(k)
        l=l+1;
        frep(l,k)=(tran1(k)-foff)/m;

    end

end topn-bottomn; yaxis=(1:(topn(1)-bottomn(1)+2))*0+130;

P12F1=[frep(:,1)-frepmin,yaxis'];
P12F2=[frep(:,2)-frepmin,yaxis'];
P32F0=[frep(:,3)-frepmin,yaxis'];
P32F1=[frep(:,4)-frepmin,yaxis'];
P32F2=[frep(:,5)-frepmin,yaxis'];

```

```

P32F3=[frep(:,6)-frepmin,yaxis'];

subplot(2,1,2)
%plot(mat(:,2),mat(:,3),mat1(:,1),mat1(:,2)*15*10^3 )
%,mat(:,1),mat(:,5))
%factor=10;

factor=1000000000000; semilogy(mat1(:,1),mat1(:,6)) axis([0 20
min(mat1(:,6)) max(mat1(:,6))]) hold on
bar(P12F1(:,1),P12F1(:,2)./factor,0.00001,'g','edgecolor','g')
%if 0
bar(P12F2(:,1),P12F2(:,2)./factor,0.0001,'r','edgecolor','r')

bar(P32F0(:,1),P32F0(:,2)./factor,0.0001,'b','edgecolor','b')
bar(P32F1(:,1),P32F1(:,2)./factor,0.0001,'y','edgecolor','y')
bar(P32F2(:,1),P32F2(:,2)./factor,0.00001,'m','edgecolor','m')

bar(P32F3(:,1),P32F3(:,2)./factor,0.00001,'c','edgecolor','c')
%bar(D52F3(:,1),D52F3(:,2)./factor,0.00001,'k','edgecolor','k')
%bar(D52F4(:,1),D52F4(:,2)./factor,0.00001,'w','edgecolor',orange)
%legend('data','P12F1','P12F2','P32F0','P32F1','P32F2','P32F3')

title('F=1')

```

Appendix E

External Cavity Diode Laser

Below I show photos of the external cavity diode laser that I built. That was my first project in the lab. Idea of operation is very simple and is described in many scientific articles.³⁹ The laser beam from the diode hits the diffraction grating. The angle of the grating is set so that the first order diffracted beam is sent back to the diode while the zeroth order is used in the experiment. External cavity diode lasers are widely used for spectroscopy, as they have very very narrow line-width and capability of wavelength tuning by changing the grating angle, which can be done by piezoelectric transducers (PZT) attached to the back side of the grating.

The laser shown below was used as a repump laser for our MOT throughout my PhD time.

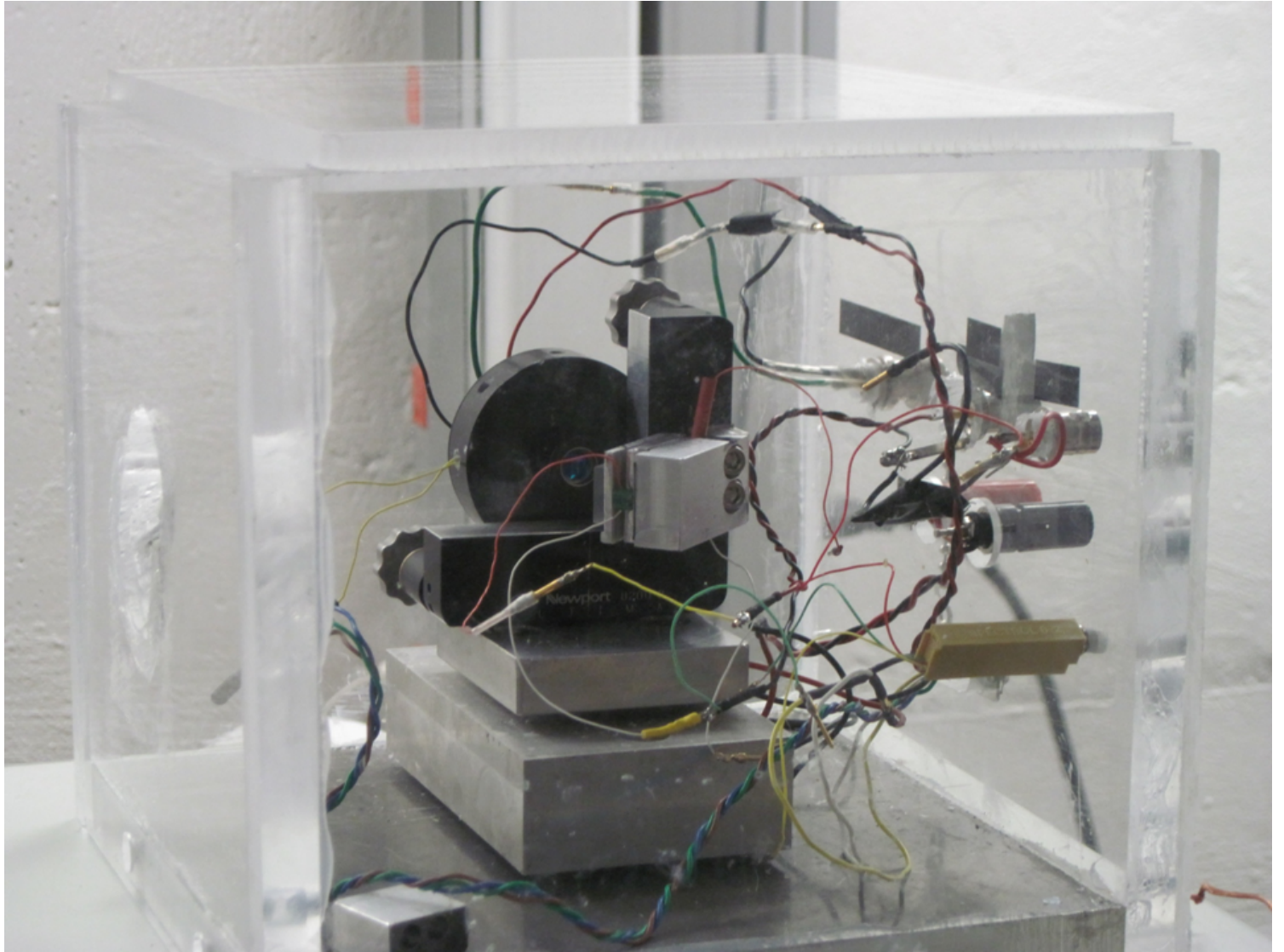


Figure E.1: *Home-made external cavity diode laser 1.*

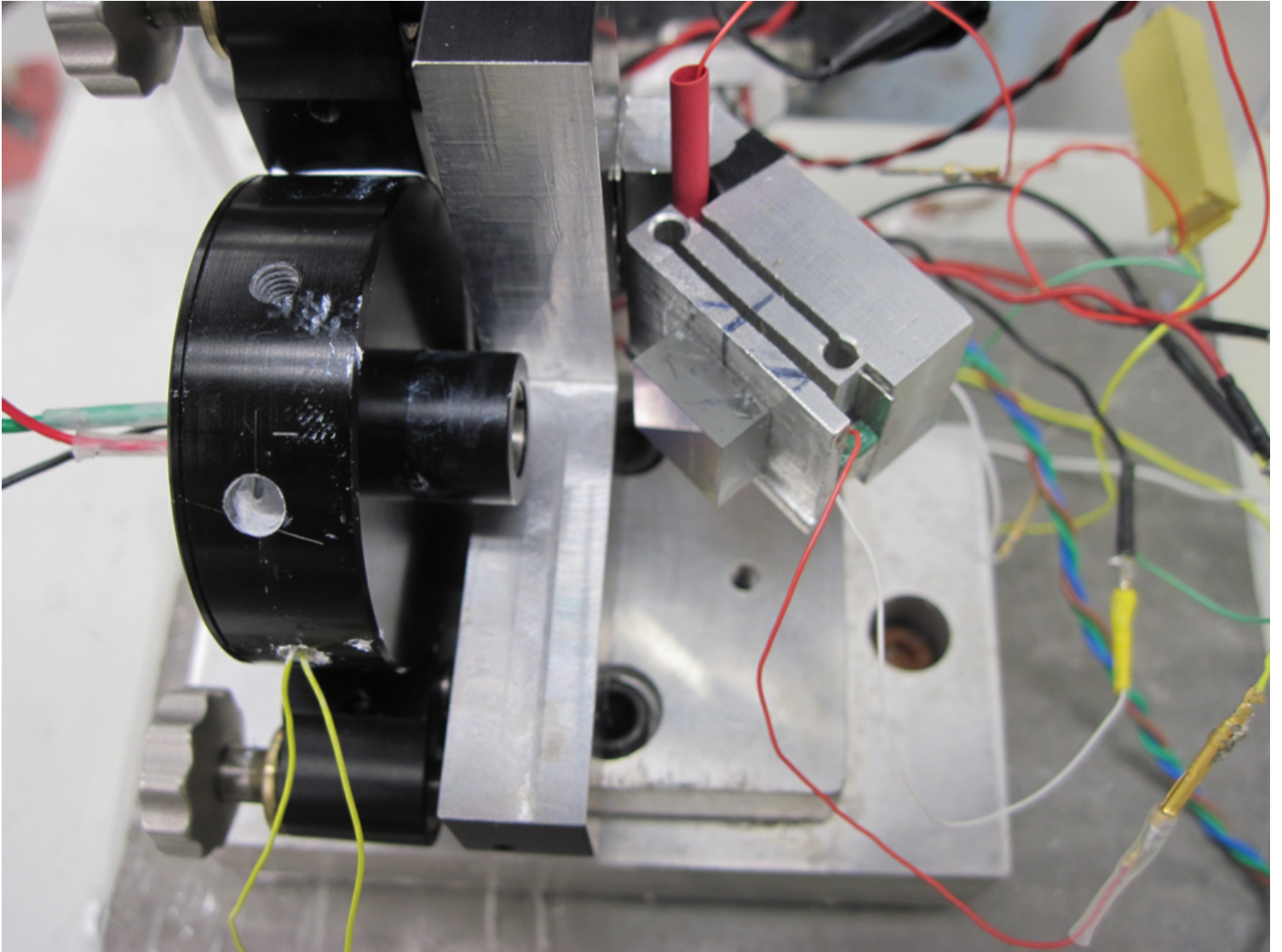


Figure E.2: *Home-made external cavity diode laser 2.*

Appendix F

Moving MOTRIMS

In addition to all the physics I have done in the J.R. Macdonald lab, including main projects (presented in this dissertation) and side projects, I spent my last period of my PhD program moving our MOTRIMS setup from one room to another and making it operational again.

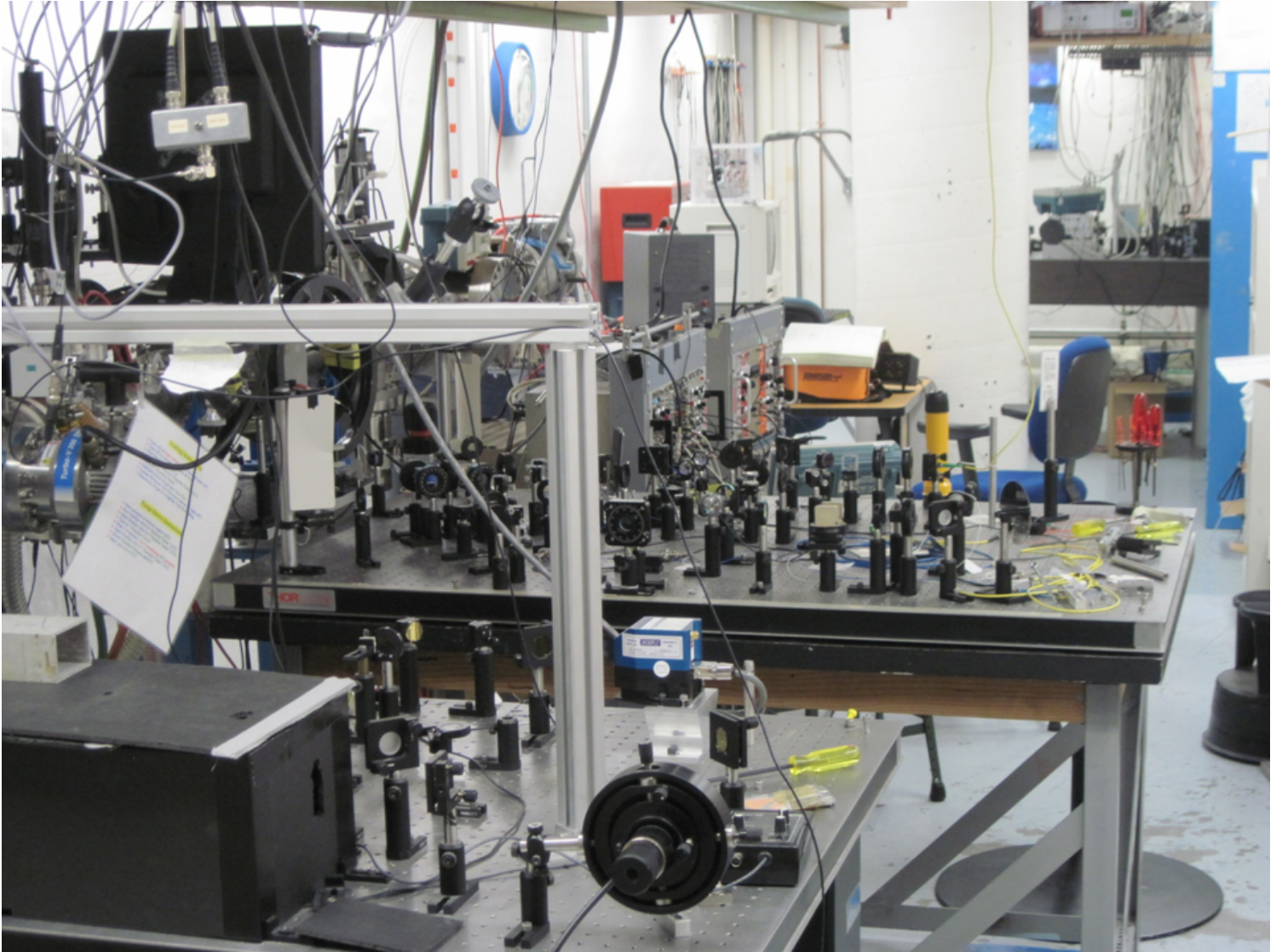


Figure F.1: *This is how the MOTRIMS apparatus looks after we moved into the new room.*